Supporting Information

Identification of Novel 'Inks' for 3D Printing Using High Throughput Screening: Bioresorbable Photocurable Polymers for Controlled Drug Delivery

Iria Louzao,[†,‡,§] Britta Koch,[†] Vincenzo Taresco,[†] Laura Ruiz-Cantu,[‡] Derek J. Irvine,[‡] Clive J. Roberts,[†] Christopher Tuck,[‡] Cameron Alexander,[†] Richard Hague,[‡] Ricky Wildman,[‡] and Morgan R. Alexander[,†]*

[†]School of Pharmacy and [‡]Faculty of Engineering, University of Nottingham, Nottingham NG7 2RD (UK).

E-mail: morgan.alexander@nottingham.ac.uk

Contents Page

S1 Poly-β-amino ester (PBAE) synthesis[1]

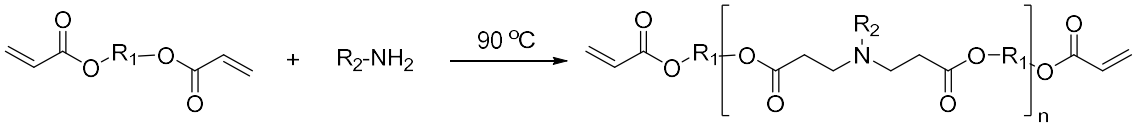

Scheme S1

Diacrylates and amines were purchased from Sigma-Aldrich or Acros and used as received. PBAE were synthesized in bulk by mixing diacrylates and amines in 1.2 molar ratio (diacrylate/amine) in scintillation vials (Scheme S1). As typical experiment, *A1* was synthesized by mixing 3.0 g (2.9 mL, 15.1 mmol) with 1.36g (1.30 mL, 12.6 mmol) of 2-(2-aminoethoxy)ethanol. Mixtures were heated at 90 °C under stirring overnight. All PBAE were synthesised at the same scale.

S2 Microarray preparation

The viscosity of pure PBAE was in general too high for piezoelectric ink jet printing; some of them were even solid at room temperature. Our strategy to reduce the viscosity of the final printable inks involved mixing with diacrylate monomers *A*-*F* (typically exhibiting viscosities between 5 and 60 cP at 25 °C) in order to meet printability requirements without compromising mechanical and degradability properties of the cured product.

Pin-printing allows for microarray preparation of a very wide range of inks for high throughput characterization of the UV cured spots.

DMF was used as a non-reactive solvent for all PBAEs in this experiment in order to study their properties in high throughput without the need to optimize viscosity in advance.

Material microarrays were prepared by combinatorial mixing of PBAE with monomers *A*-*G* and printed as spots of 300 μm average diameter followed by photo polymerization. PBAE were dissolved in 75% DMF (w/v) by mechanical stirring overnight. Monomers and PBAE solutions were mixed in 1:1 volume ratio. From the 312 possible new copolymers, the study

covers 253, since 6 of the 42 PBAE were not soluble at 75% DMF (w/v), preventing ready contact printing. Monomer/PBAE solutions containing all of them 2% (w/v) of 2,2-dimethoxy-2- phenylacetophenone (DMPA) as photoinitiator were transferred to untreated glass slides by using XYZ3200 dispensing station (Biodot) and metal pins (946MP6B, Arrayit) under argon atmosphere (< 2000 ppm oxygen) and between 40 and 50% humidity. The spots were UV polymerized under argon atmosphere for 10 min after printing.

For drug release experiments, 5 μL of those mixtures containing paroxetine hydrochloride were manually pipetted into oxygen-etched (in order to prevent eventual detaching of the materials from the plate surface) 384 polypropylene well plates. Final paroxetine hydrochloride concentration was 20 ng/μL. Then, the plates were exposed to UV for 20 minutes under an argon atmosphere.

Both the glass slides and the plates were dried in a vacuum oven to remove the solvent for one week.

Table S1. PBAE and corresponding derived materials derived included in the high-throughput experiments.

PBAE Code	***Acrylate Identity***	***Amine Identity***	***Acrylate-to-Amine Ratio***	***Derived materials[a]***
A1	A	1	1.2	*AA1, BA1, CA1, DA1, EA1, FA1, GA1*
A2	A	2	1.2	*AA2, BA2, CA2, DA2, EA2, FA2, GA2*
A3	A	3	1.2	*AA3, BA3, CA3, DA3, EA3, FA3, GA3*
A4	A	4	1.2	*AA4, BA4, CA4, DA4, EA4, FA4, GA4*
A5	A	5	1.2	*AA5, BA5, CA5, DA5, EA5, FA5, GA5*

B2	B	2	1.2	*AB2, BB2, CB2, DB2, EB2, FB2, GB2*
B3	B	3	1.2	*AB3, BB3, CB3, DB3, EB3, FB3, GB3*
B5	B	5	1.2	*AB5, BB5, CB5, DB5, EB5, FB5, GB5*
C1	C	1	1.2	*AC1, BC1, CC1, DC1, EC1, FC1, GC1*
C2	C	2	1.2	*AC2, BC2, CC2, DC2, EC2, FC2, GC2*
C3[b]	C	3	1.2	*AC3, BC3, CC3, DC3, EC3, FC3, GC3*
C3-12[b]	C	3	1.2	*AC3-12, BC3-12, CC3-12, DC3-12, EC3-12, FC3-12, GC3-12*
C3-15	C	3	1.5	*AC3-15, BC3-15, CC3-15, DC3-15, EC3-15, FC3-15, GC3-15*
C3-2	C	3	2.0	*AC3-2, BC3-2, CC3-2, DC3-2, EC3-2, FC3-2, GC3-2*
C4	C	4	1.2	*AC4, BC4, CC4, DC4, EC4, FC4, GC4*
C5	C	5	1.2	*AC5, BC5, CC5, DC5, EC5, FC5, GC5*
C6	C	6	1.2	*AC6, BC6, CC6, DC6, EC6, FC6, GC6*

C7	C	7	1.2	*AC7, BC7, CC7, DC7, EC7, FC7, GC7*
C8	C	8	1.2	*AC8, BC8, CC8, DC8, EC8, FC8, GC8*
C9	C	9	1.2	*AC9, BC9, CC9, DC9, EC9, FC9, GC9*
D1	D	1	1.2	*AD1, BD1, CD1, DD1, ED1, FD1, GD1*
D2	D	2	1.2	*AD2, BD2, CD2, DD2, ED2, FD2, GD2*
D3	D	3	1.2	*AD3, BD3, CD3, DD3, ED3, FD3, GD3*
D5	D	5	1.2	*AD5, BD5, CD5, DD5, ED5, FD5, GD5*
E1	E	1	1.2	*AE1, BE1, CE1, DE1, EE1, FE1, GE1*
E3	E	3	1.2	*AE3, BE3, CE3, DE3, EE3, FE3, GE3*
F1	F	1	1.2	*AF1, BF1, CF1, DF1, EF1, FF1, GF1*
F2	F	2	1.2	*AF2, BF2, CF2, DF2, EF2, FF2, GF2*
F3	F	3	1.2	*AF3, BF3, CF3, DF3, EF3, FF3, GF3*
F6	F	6	1.2	*AF6, BF6, CF6, DF6, EF6, FF6, GF6*

[a] Diacrylate A-F and PBAE were mixed at 1:1 v/w ratio. [b]*C3* and *C3-12* represent different batches.

S3 Screening for drug release kinetics

The wells were incubated in 100 μL of phosphate buffered saline (PBS, pH 7.4) and at due time points, 75 μL were transferred to plates suitable for fluorescence measurements and replenish with fresh PBS by using a liquid handling system (Precision XS, Biotek). The fluorescence was measured by using a Tecan plate reader at an excitation wavelength of 270 nm (± 20 nm) and the emission was measured between 315 and 400 nm. The emission intensity at 335 nm was used for analysis. Every well contained 100 ng of drug. The experiments were performed in triplicate and including a control plate containing the (co)polymers without drug to subtract the background.

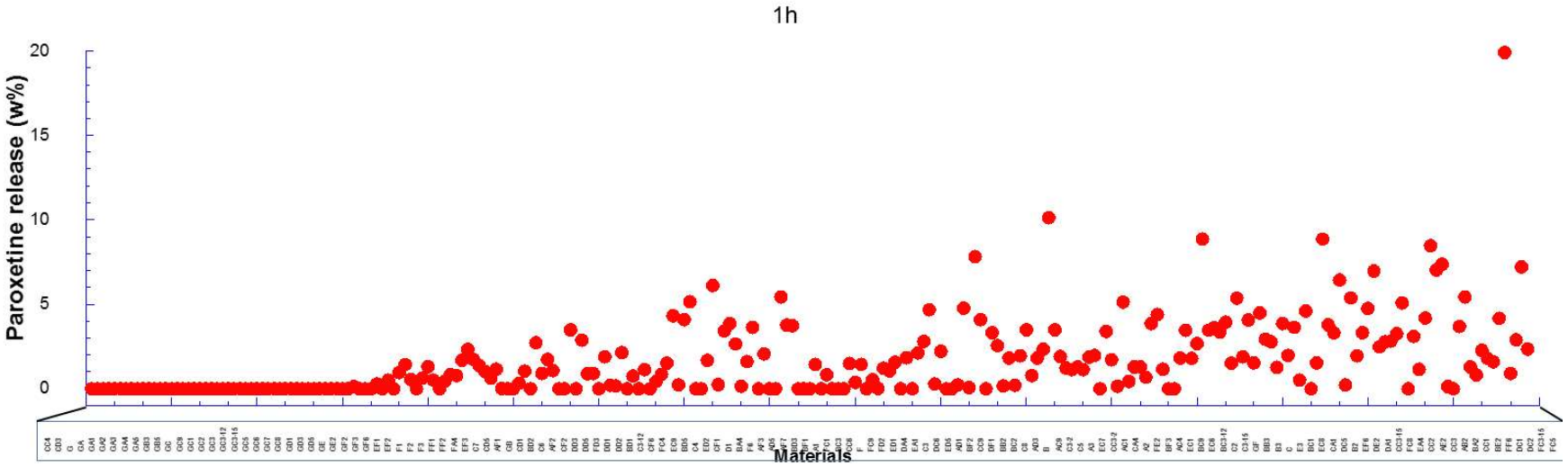

Figure S1. Cumulative paroxetine release in weight percentage after 1h of incubation with PBS. Materials are ordered from lower (left) to higher (right) release at 20h.

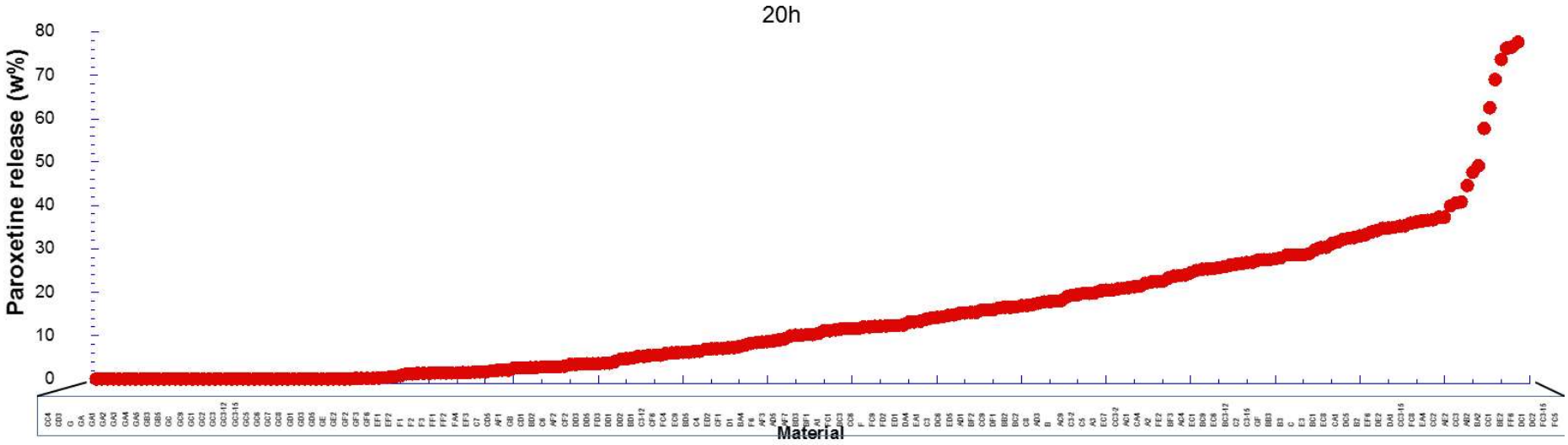

Figure S2. Cumulative paroxetine release in weight percentage after 20h of incubation with PBS. Materials are ordered from lower (left) to higher (right) release.

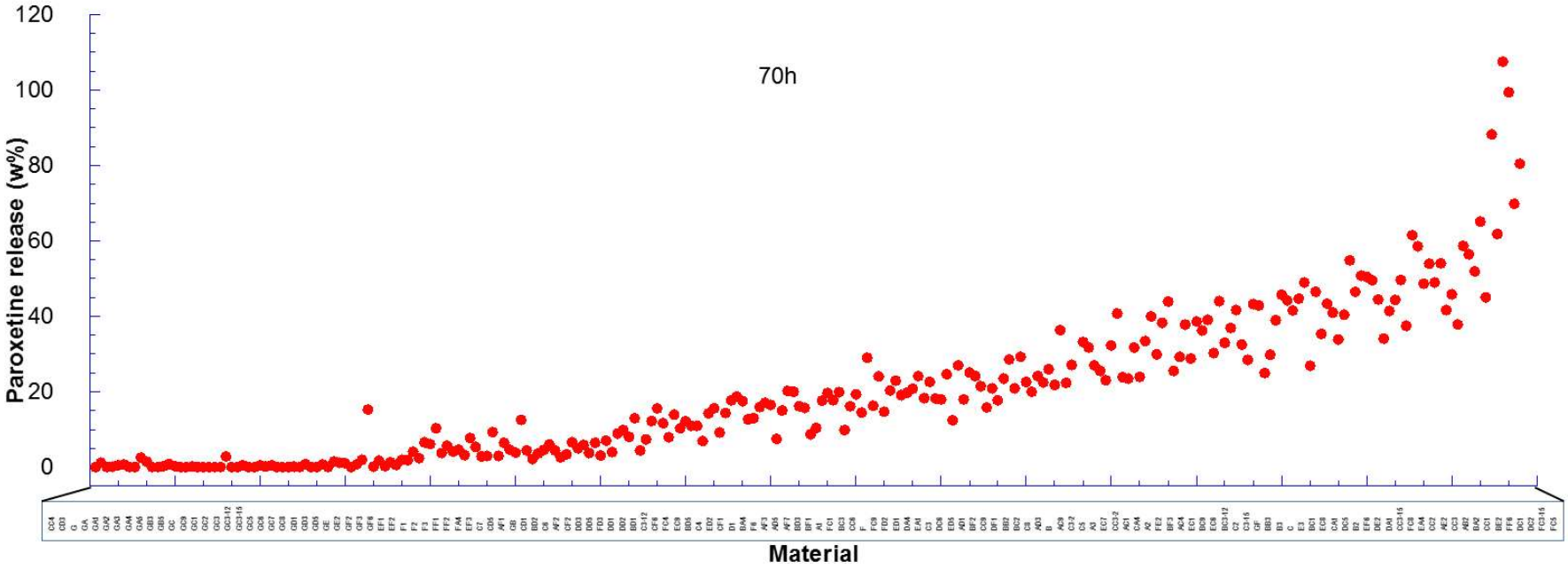

Figure S3. Cumulative paroxetine release in weight percentage after 70h of incubation with PBS. Materials are ordered from lower (left) to higher (right) release at 20h.

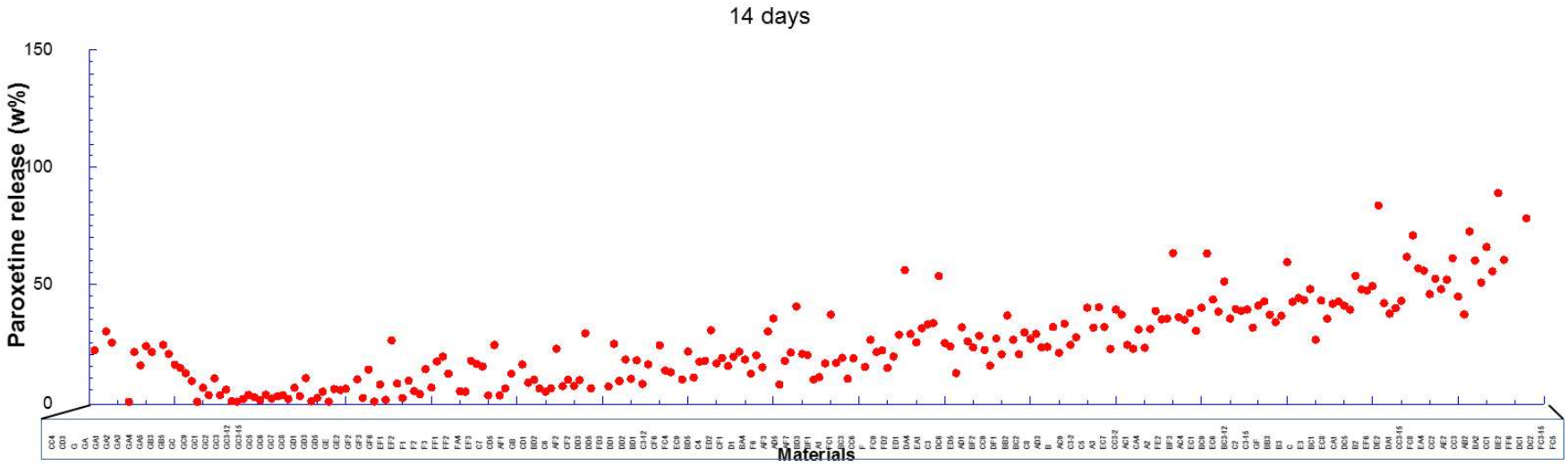

Figure S4. Cumulative paroxetine release in weight percentage after 14 days of incubation with PBS. Materials are ordered from lower (left) to higher (right) release at 20h.

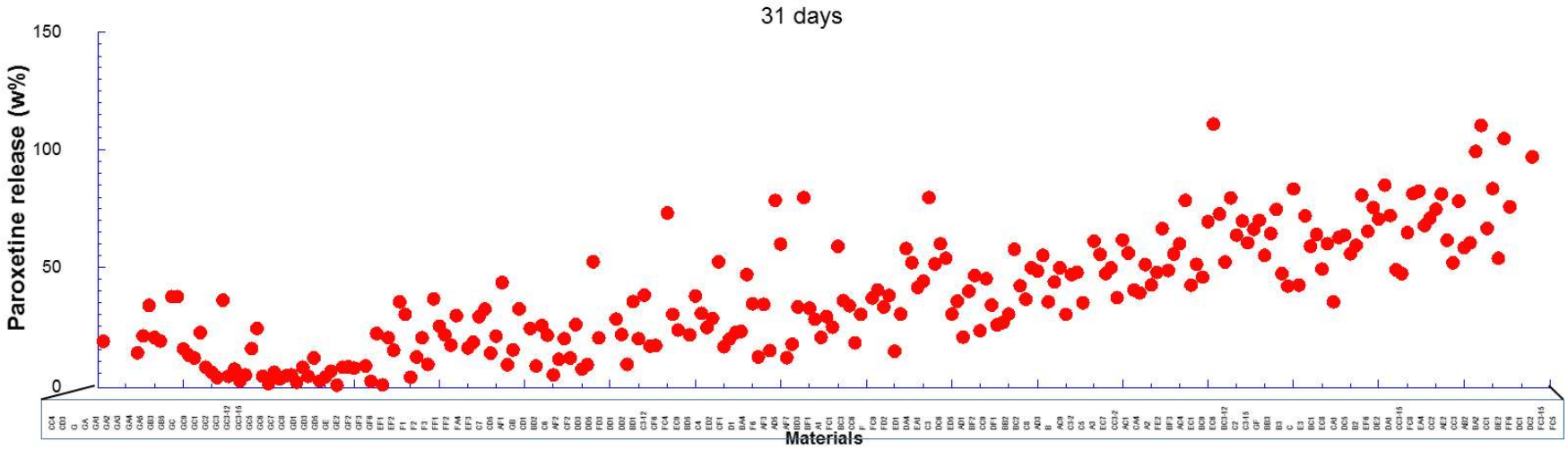

Figure S5. Cumulative paroxetine release in weight percentage after 31 days of incubation with PBS. Materials are ordered from lower (left) to higher (right) release at 20h.

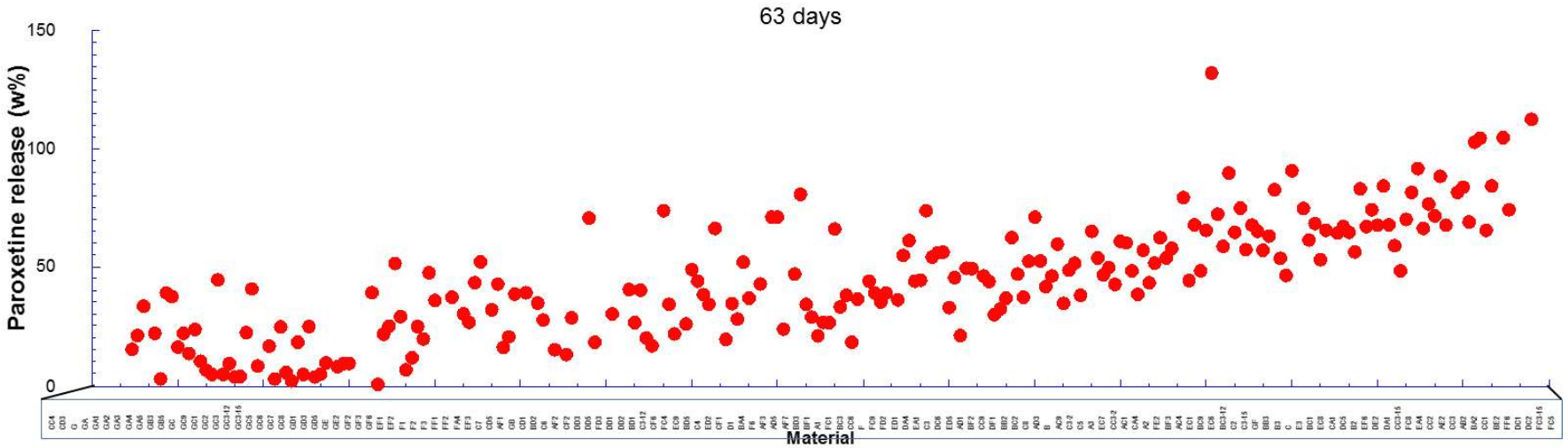

Figure S6. Cumulative paroxetine release in weight percentage after 63 days of incubation with PBS. Materials are ordered from lower (left) to higher (right) release at 20h.

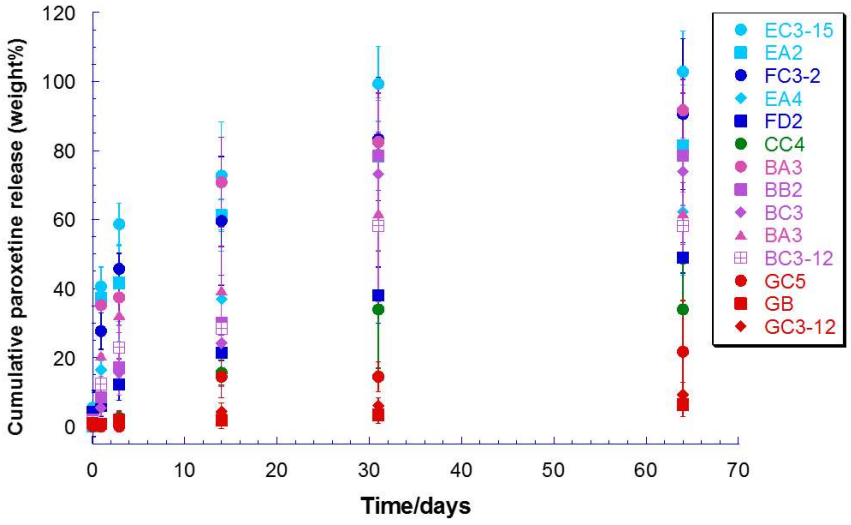

Figure S7. Cumulative kinetic release profile for 10 of the hit materials, colour coded by diacrylate composition: ethylene glycol (blue), propylene glycol (green), hydrophobic and aromatic (purple) and phenolic methacrylamide (red) over 31 days.

S4 Atomic Force Microscopy

Height, Peak Force error, DMT modulus, logDMT modulus, adhesion, deformation and dissipation images were simultaneously acquired by Peak Force QNM-AFM measurements (Bruker Fast Scan). 3 images of 5x5 μm per spot were recorded by using a programmable stage.[2] 2 different cantilevers of different stiffness nominal k= 40 (RTESPA 300) and 3 N/m (RFESPA MPP-21120) were used to cover most of the material moduli. Poisson's ratio of 0.3 has been applied in all cases. Three images were acquired per polymer spot throughout the micro array. Actual spring constant was estimated by thermal tune.

The geometrical models applied to estimate elastic modulus are not trivial[3–6] and all have assumptions which can lead to different levels of uncertainties. The deformation values are related to the indentation of the tip probe into the material and these values determine the geometrical model to be used to estimate the elastic modulus. Since the deformation values

cover a wide range, single point AFM force-distance curve measurements were additionally performed for some of the materials by using the same type of probes together with measurements of standard materials, including polystyrene (PS, 1GPa) and low density polyethylene (LDPE, 150 kPa) (supplied by the National Physical Laboratory, UK). With these data and tip shape measurements, the QNM DMT modulus has been corrected. The actual geometry of the AFM tip is not coincident with the theoretical models, and average parameters were used to correct the data together with the wide range of deformation associated to elastic modulus throughout the array. Materials showing differences of more than one order of magnitude between three replicates or between the two microarray datasets have been omitted due to the high degree of uncertainty in the measurements (78 of 253).

Several sets of force curve measurements[7,5] with the same type of probes were done for 7 representative materials by using two types of probes. The trigger threshold was selected according to a setpoint which gives a deformation in QNM between 10 and 20 nm. Different scan rates were also varied, since PeakForce QNM data was acquired at 2 kHz rate. Tip shape measurements were performed by using TGT1 substrates. According to those experiments a half cone angle of 80 degrees and a radius of 312 nm was used to apply “cone”, “cylinder” or “sphere” models to calculate elastic moduli. All those results for every sample were analysed (Analysis worksheet implemented in Microsoft Excel, Dr. Xinyong Chen, University of Nottingham) and compared with the results obtained by automation. The differences between the results obtained by Peak Force and force curve measurements were used to correct and set the intervals of elastic moduli. Sample standards of polystyrene (PS) and low density polyethylene (LDPE) of 1.6 GPa and 100 MPa elastic moduli respectively were also used to validate tip characterization.

S5 Screening for PBAE-array cytotoxicity

Cytotoxicity of PBAE was tested on immortalized human mesenchymal stem cells (hMSCs) according to an adapted protocol for agar diffusion cell culture screening of macroscopic biomaterial samples.[8] Briefly, immortalized JCRB1149 [UE6E7T-11] human mesenchymal stem cells (JCRB Cell Bank, Japanese Collection for Research) were grown in high-glucose DMEM (Gibco) supplemented with 10% FBS (Sigma-Aldrich), 1x L-glutamine (100x, Gibco), 1x penicillin/ streptomycin (100x, ThermoFisher Scientific) and 1 vol% non-essential amino acid solution (NEAA, Invitrogen) and were maintained in a humidified incubator (37 °C, 5% CO_2). For the experiments, cells were detached using trypsin–EDTA solution (0.25%; Sigma) and resuspended in fresh medium to seed a final concentration of 10^6 cells per 6 cm Petri dish. After allowing the cells to settle at room temperature they were grown for 24 h in a humidified incubator to yield a confluent cell monolayer. For the agar diffusion assay the medium in each Petri dish was removed and the cell monolayer washed once with PBS. Next, 1 mL of an autoclaved and molten 3% (weight/volume) Noble agar (Sigma) solution in PBS was mixed with 2 mL of cell culture medium at 39 °C. This mixture was then quickly added to the cell layer and evenly distributed by rotating the dish, resulting in an approximately 0.4 cm thick layer. After solidification of the agar layer at room temperature the samples were equilibrated in a humidified incubator for 15 min before placing a UV-sterilized PBAE microarray sample on top of the agar layer with the polymer spots facing towards the cells. As a known cytotoxic polymer control, cyanoacrylate adhesive (Super Glue, Loctite) spots on a glass slide of a comparable size were tested in a separate Petri dish. Similarly, bare and polyHEMA-coated glass were employed as negative controls. The position of the samples with respect to fiducial pen marks at the bottom of the Petri dishes was imaged with a Leica DM IRB/E inverted microscope (imaging software: Volocity Version 6.0.1, PerkinElmer 2011; objective: 5x/0.12 NPlan). After incubating the samples for the designated time (48 h)

in a humidified incubator, the glass slides were carefully removed, 0.5 mL of Neutral Red solution (Sigma) added and the Petri dishes returned for another 1 h to the incubator. Neutral Red accumulates in the lysosomes of viable cells and is therefore commonly used as a dye in cytotoxicity assays where cell viability is assessed. [9] The agar layer was then carefully removed by tilting the samples and detaching the agar from the rim of the dishes. PBS was added and brightfield images of the stained cell monolayer as well as the position of the fiducial marks were taken in brightfield mode.

Image post-processing involved stitching of the acquired tiles with the 'Grid/Collection stitching plugin'[10] in ImageJ (Version 1.51f, 64 bit), manual alignment of the cell and microarray sample images with the help of the fiducial marks ('Align Image by line region of interest (ROI)'-plugin), intensity inversion (so that higher intensity corresponds to higher neutral red staining) and analysis in CellProfiler2.2.0. Both the area covered by cells and the staining intensity were quantified from the binary and reverted image, respectively, in circular regions of interest with diameter d = 1 mm. Normalized cell viability was calculated as the neutral red intensity per cell area.

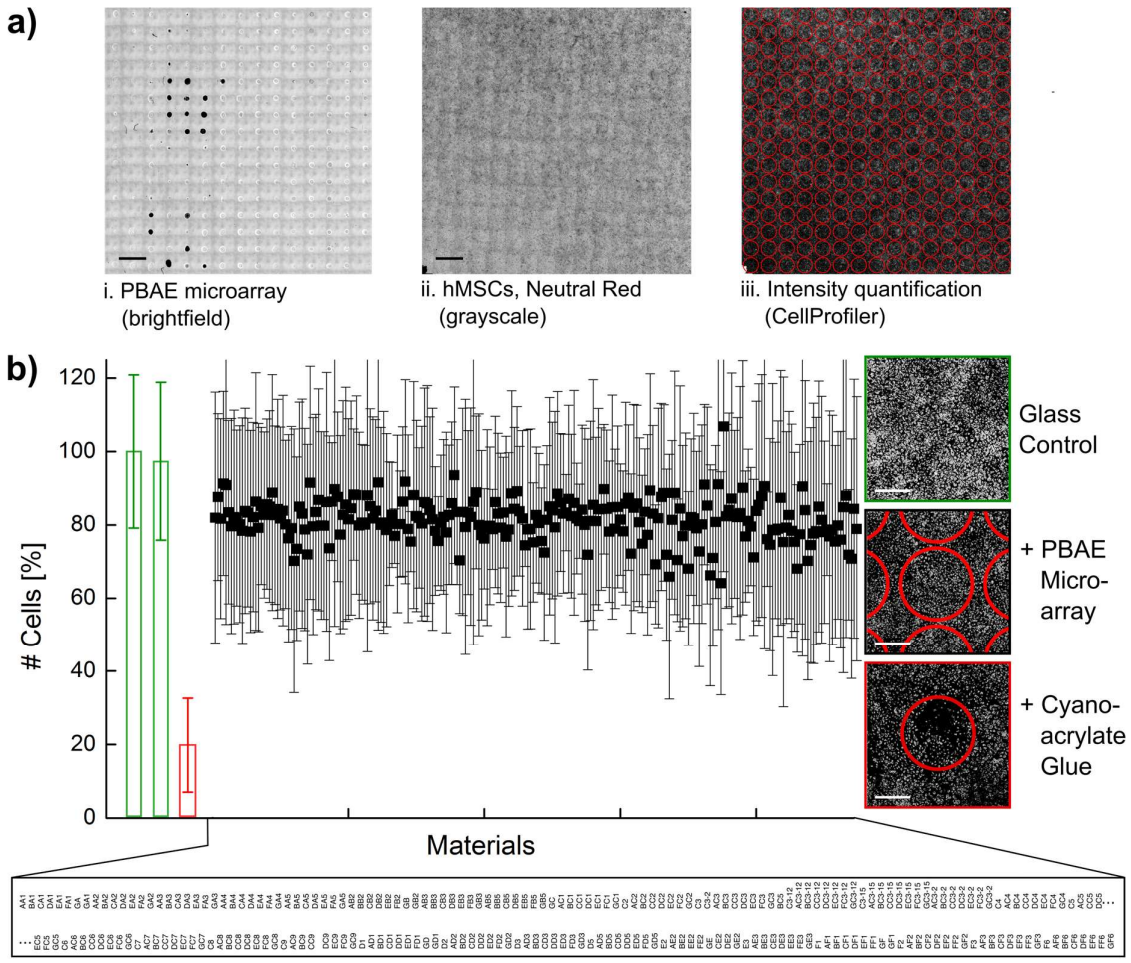

Figure S8. Cytotoxicity assessment for PBAEs in a high-throughput microarray format. (a) (i) Stitched brightfield images of the PBAE microarray and (ii) hMSC cell layer after PBAE incubation and Neutral Red staining. (iii) Image ii. after intensity inversion (for quantification purposes) with an overlay of the regions of interest (ROI, red circles) of 1 mm. (b) Number of cells quantified from the Neutral Red stain for the PBAE materials. Green bars show negative controls (left to right: bare glass and pHEMA-coated glass), the red bar the positive control (cyanoacrylate adhesive). Insets to the right show exemplary ROIs for (top to bottom) negative control, PBAE array, cyanoacrylate adhesive. Red circles indicate positions of polymer spots. Scale bars equal (a) 2 mm and (b) 0.5 mm, respectively.

S6 Screening for printability

Printability screening was performed using a piezo electric microarray printer (SciFlexarrayer S5 Scenion). The inks were prepared at 6.25%, 12.5%, 25% and 50% in DMF and 50 µl of each solution was transferred into 384 well plate. The printer was programed to aspirate 10 µl of the material and deposited 100 droplets to form each spot. Nine spots of each material concentration were deposited onto a glass slide. The voltage and pulse were modified for each material before deposition until the limits were reached. Images of the drop formation and droplet size were obtained using the printer software. The final spots were imaged using the Leica MZ16 stereomicroscope. The two parameters that were taken into account to decide if a material was printable were aspiration and deposition (Figure S9 and Table S2).

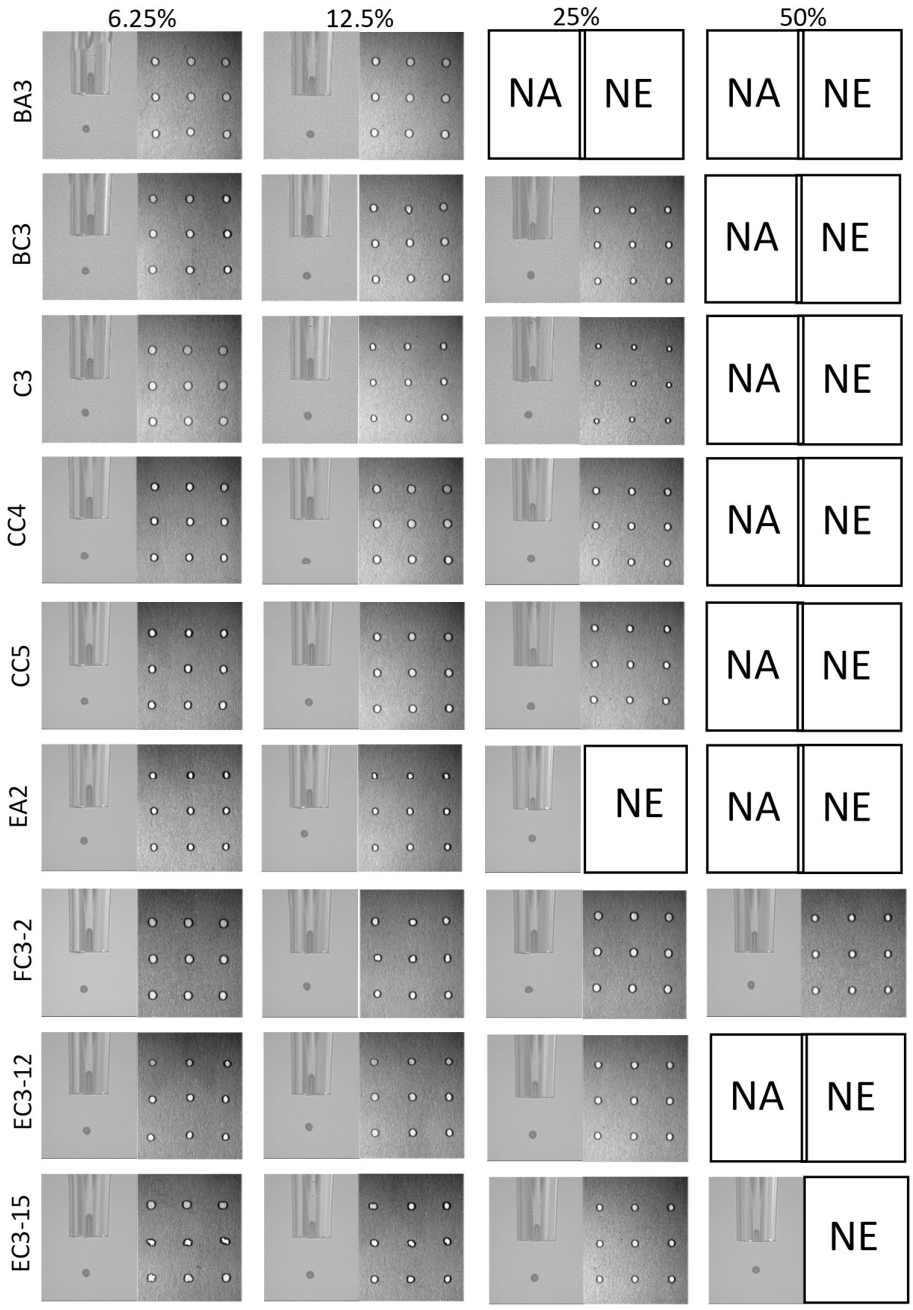

Figure S9. Printability screening of hit materials at different concentrations in DMF. NA= no aspirated, NE= no ejected.

Table S2. Voltage (V), pulse (P) and drop volume (DP) for each material at the different concentrations.

ink %	6.25%			12.50%			25%			50%		
ink	V	P	DP (pL)	V	P	DP (pL)	V	P	DP (pL)	V	P	DP (pL)
BA3	78	50	186	84	50	214	NP	NP	NP	NA	NA	NP
BC3	78	50	189	85	50	215	93	50	208	NA	NA	NP
C3	78	50	188	85	50	202	99	50	198	NA	NA	NP
CC4	78	50	202	85	50	223	86	50	209	NA	NA	NP
CC5	78	50	186	82	50	208	93	50	224	NA	NA	NP
EA2	78	50	185	78	50	168	120	50	NP	NA	NA	NP
FC3-2	78	50	198	85	50	202	90	50	208	93	50	196
EC3-12	78	50	210	78	50	186	93	50	210	NA	NA	NP
EC3-15	78	50	212	78	50	186	93	50	210	120	58	NP

S7 3D Printing

A commercial inkjet printer (Dimatix DMP 2800, Fujifilm, Santa Clara, CA, USA) equipped with cartridges of 10 pL nominal droplet volume and 21.5 µm nozzle size (Dimatix Materials Cartridges) involving a microelectromechanical system (MEMS) jetting structure was used to print the scaled-up ink formulations. All inks were prepared at 1.5 mL scale by bubbling a nitrogen flow for 15 min for degassing and kept in the dark overnight. Standard, not optimized waveforms were used for printing.[11] The printer was placed in a glovebox under nitrogen atmosphere (< 2% oxygen). The printhead was connected to a UV LED (365 nm, 3.5 J/cm2) to allow for UV curing while printing. Different objects following different patterns were printed at 3 kHz jetting frequency by using 6 nozzles (35 µm drop spacing) simultaneously on polyethylene terephtalate (PET) due to the convenient detachment of the printed objects.

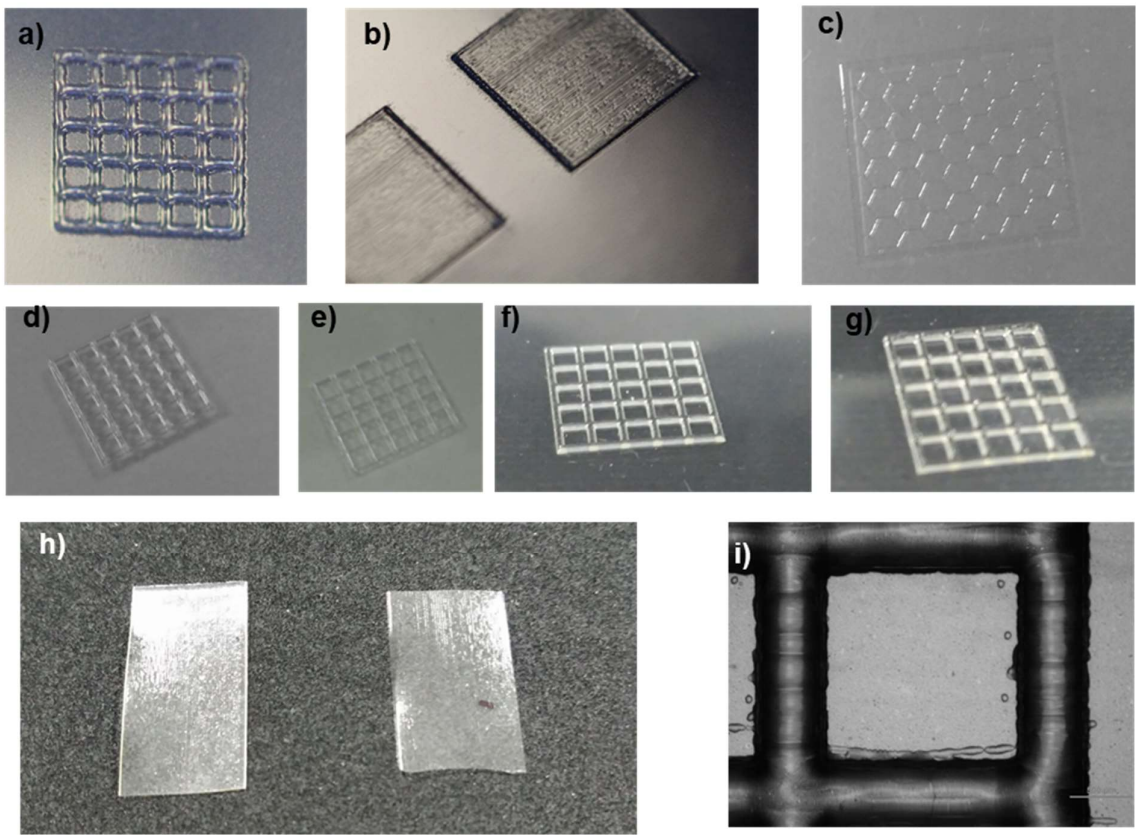

Figure S10. Representative pictures (a-h) and micrograph (i) of printed objects by using *FC3-2* ink: (a, d, f, g, i) 5x5 mm 99 and (e) 50-layer grid, (b) 1x1 cm 25-layer squares, (c) 1x1 cm 5-layer honeycomb-like object and (h) two pieces of a rectangle (10x25 mm, 25 layers, average thickness 137 μm) after tensile experiments were carried out. Scale bar: 500 μm.

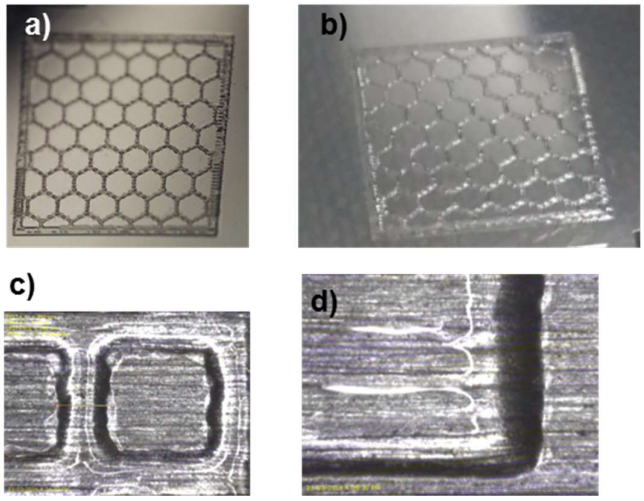

Figure S11. Representative pictures (a-d) of printed objects by using *EC3-15* ink: (a,b)1x1 cm 5-layer honeycomb, (c) 5x5 mm 10-layer grid and (d) 25-layer square.

S8 Rheology and surface tension measurements

A Malvern Kinexus Pro Rheometer equipped with a parallel plate at 400 µm separation, was used for viscosity measurement under shear rates from 10 s^{-1} and 1,000 s^{-1}. Each measurement started at 25°C with 5°C increments up to 70°C. The viscosity was recorded at 5 s intervals within a 180 s test time at each temperature point and shear rate.

A Kruss DSA100S was used for the determination of surface tension at room temperature, applying the pendant drop method and using the Young–Laplace equation.

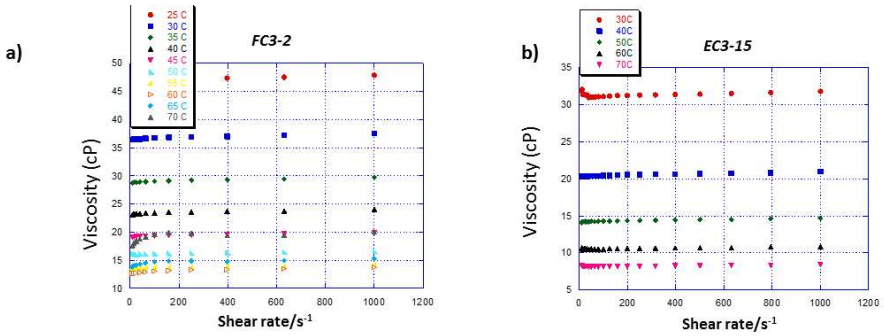

Fig. S12. Viscosity (cP) against shear rates (s^{-1}) at different temperatures of the scaled up inks (a) *FC3-2* and (b) *EC3-15*.

S9 Drug release of printed materials

For drug release experiments, PBS was added to scintillation vials containing the printed materials squared samples (5 replicates) weighing between 16.4 and 17.0 mg to reach a ratio of 10 mg sample/mL of PBS. At due time points, 500 µL were withdrawn from the vials and replenished by fresh PBS. The withdrawn amount was placed into vials and analysed by HPLC equipped with a fluorescence detector (λ_{ex}= 294 nm, λ_{em} = 330 nm). Phosphate buffer 25mM pH 2.5 and acetonitrile (66/33)[12] was used as eluent in isocratic mode (0.8 mL/min) in a C18 Jupiter analytical column (Phenomenex). The injected volume was 15 µL.

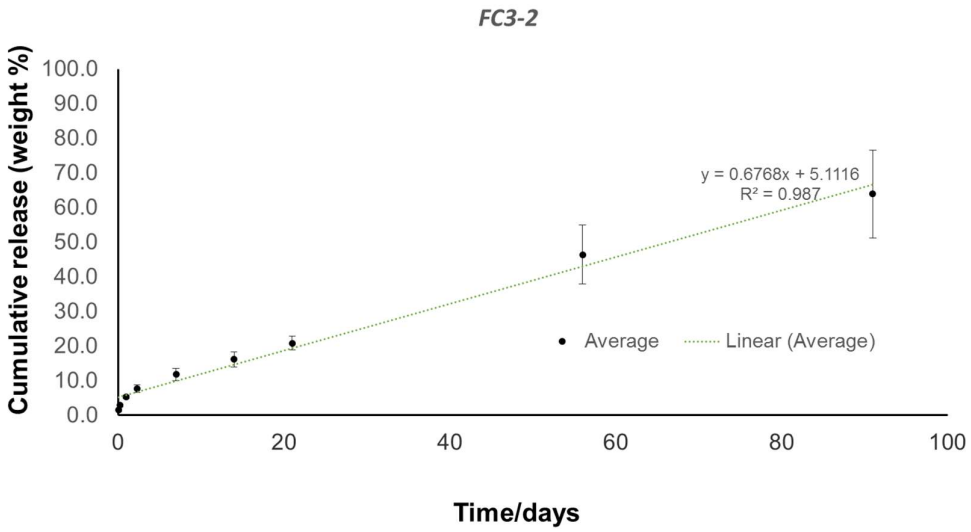

Fig. S13. Linear fitting of the cumulative release of paroxetine in printed 25x25 mm squares printed (average of 5 replicates, 25 layers, average thickness 113 μm).

S10 Degradability experiments by dissolution

Printed squared materials (25 layers, 5 replicates) were freeze dried prior to immersion in 10 mL PBS at 37C. At due time points, materials were briefly washed with deionized water to remove salts from the buffer and freeze dried at certain time intervals and weighed to calculate the weight loss. Starting sample weights were 17.0, 16.5, 16.8, 17.5 and 17.4 mg respectively.

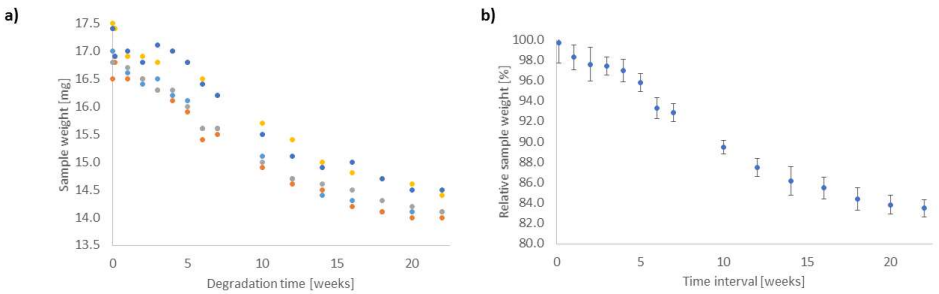

Figure S14. Weight loss over time. (a) Weight of printed squares after immersion in PBS and freeze-drying. Every individual replicate is identified with different colors. (b) Relative weight loss over time (5 replicates). Error bars depict standard deviation.

S11 Tensile tests

Tensile tests of printed objects were conducted on a TA.XTplus Texture Analyser with a load cell of 5 kg, using pneumatic clamps to secure the samples. The tests were performed in samples measuring 25 x 10 x 0.137 mm (length/width /thickness) at 20 mm/min (4 replicates). Strain, stress and the Young's modulus values were obtained.

S12 Time of Flight-Secondary Ion Mass Spectrometry (ToF-SIMS)

Measurements were conducted in a ToF-SIMS IV (IONTOF GmbH) instrument using a bismuth (Bi+) ion gun source.

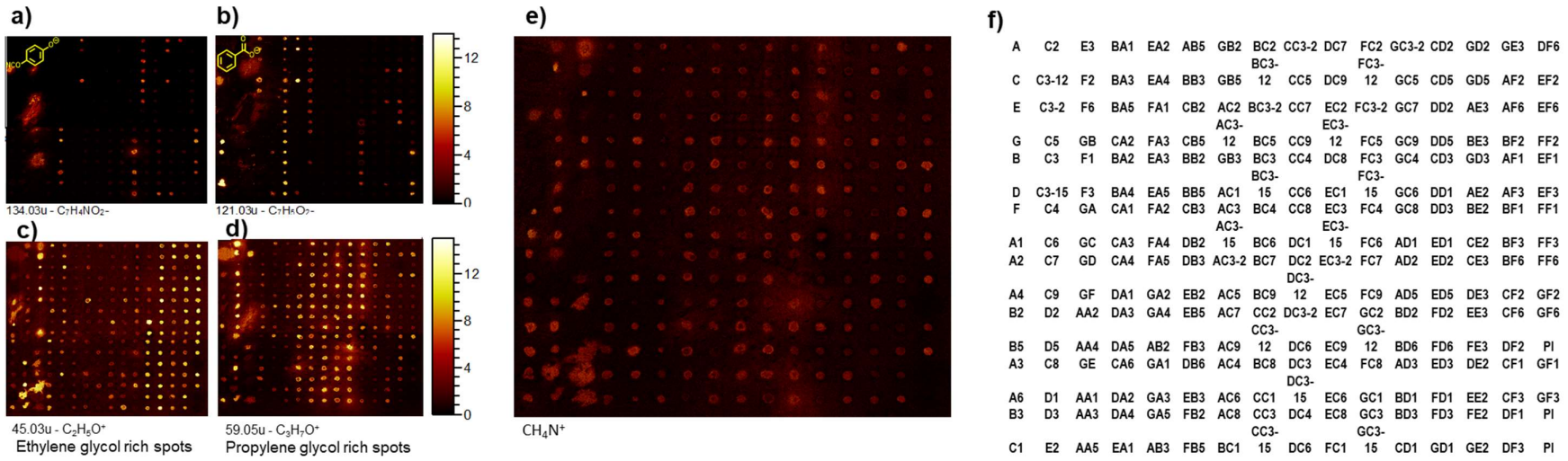

Figure S15. Representative ion intensity images of a full spot microarray. (a) Negative mode images showing the intensities of a characteristic ion of monomer *G* depicted at the top left corner and (b) benzoate anion characteristic of monomer *B*. (c) Positive mode images showing the intensities of characteristic ions of ethylene glycol rich diacrylates (*D*, *E*, *F*) and (d) propylene glycol rich diacrylate (*C*). The light colour depicts higher number of counts (higher intensity) as represented by the bars at the right. (e) Positive mode image showing the intensities of CH_4N^+, characteristic of amine and amide functional groups. The absence of this ion on the material spots containing just diacrylates (*A*-*F*) and on the spots containing just the photoinitiator in DMF indicate the removal of the DMF solvent. All other spots exhibit CH_4N^+ because of their content of PBAE or monomer methacrylamide *G*. (f) Material identification is provided by a microarray map where PI represents control spots involving only photoinitiator (2,2-dimethoxy-2-phenylacetophenone) in DMF, which not surprisingly also exhibits $C_7H_5O_2^-$ when unreacted (b).

S13 Gel Permeation Chromatography (GPC)

GPC was performed on an Agilent GPC with RI detector. Separations were performed on series of PLgel mixed bed (D) columns (250 x 4.6 mm, 5 µm bead size) fitted with a matching guard column (PLgel, 50 x 4.6 mm). The mobile phase was chloroform at a flow rate of 1.0 mL/min. Molecular weights were calculated based on a standard calibration method using poly(methyl methacrylate) (PMMA) narrow standards (M_n range: 1,800,000-505 g mol^{-1}).

Table S3. Molecular weight distribution (M_n and M_w) of pure PBAE in Da and polydispersity (M_n/M_w) calculated by GPC or M_n estimated by ^{1}H NMR. The degree of polymerization (DP) was estimated by ^{1}H NMR in all cases. M_n was estimated

PBAE	M_n/Da (DP_{NMR})[a]	M_w/Da	M_w/M_n
A1	2900±290 [a] (9)[b]	-	-
A2	2900±290[a] (10)[b]	-	-
A3	970±100[a] (3) [b]	-	-
A5	1000±100[a] (3) [b]	-	-
B2	2319±276[c] (4) [b]	3539±422	1.5
B3	2245±268 [c] (6) [b]	3231±385	1.4
C1	1880±224[c] (4) [b]	2809±335	1.5
C2	3400 ±340[a](8-9)[b]		
C3-15	1341±160[c] (3) [b]	2758±329	2.8
C3-2	660±70[a] (1) [b]	-	-
C4	1000 ±100 [a] (2) [b]	-	-
C5	2212±264[c] (4-5) [b]	3367±401	1.5
C6	1900±190[a] (4) [b]	-	-
C7	5000±500[a] (11) [b]	-	-
C8	3800±380[a] (9) [b]	-	-
C9	3200±320[a] (7-8)[b]	-	-
D1	11000±1100[a](25) [b]	-	-
D2	3769±449[c] (6) [b]	6051±721	1.6
D3	2991±356[c] (4) [b]	4613±550	1.5
D5	3500±350[a] (9) [b]	-	-
E2	800±100[c] (2) [b]	1900±200	2.4
E3	800±200[a] (2) [b]	-	-
F1	1500±150 (5)[a] [b]	-	-
F2	6000±600[a] (11) [b]	-	-
F3	3500 ± 350[a] (6) [b]	-	-

[a] Mn estimated by ^{1}H NMR (10% error) [b] Degree of polymerization estimated by ^{1}H NMR comparing signals from the acrylate and from the amine at chemical shifts appropriate for individual integration. [c]Estimated by GPC.

S14 Nuclear Magnetic Resonance (NMR) Spectroscopy

NMR spectra were recorded on a Bruker 400 MHz spectrometer. Chemical shifts are reported in ppm (δ units) downfield from the residual $CDCl_3$ signal (7.26 ppm) both for ^1H NMR spectra and ^{13}C NMR spectra (100 MHz, 77 ppm). The integrals used to calculate de DP are shown. In the cases where the Mn was estimated by NMR , the signals are also shown.

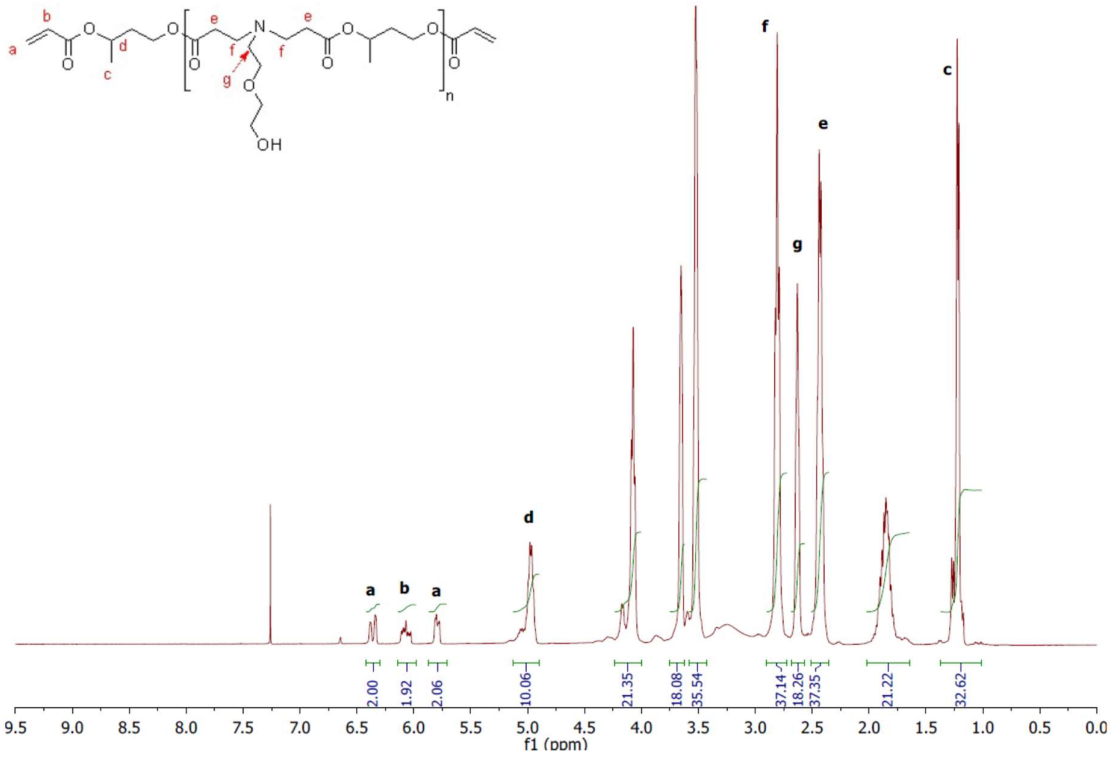

Figure S16. ^1H NMR spectrum ($CDCl_3$, 400 MHz) of PBAE *A1* (n=9).

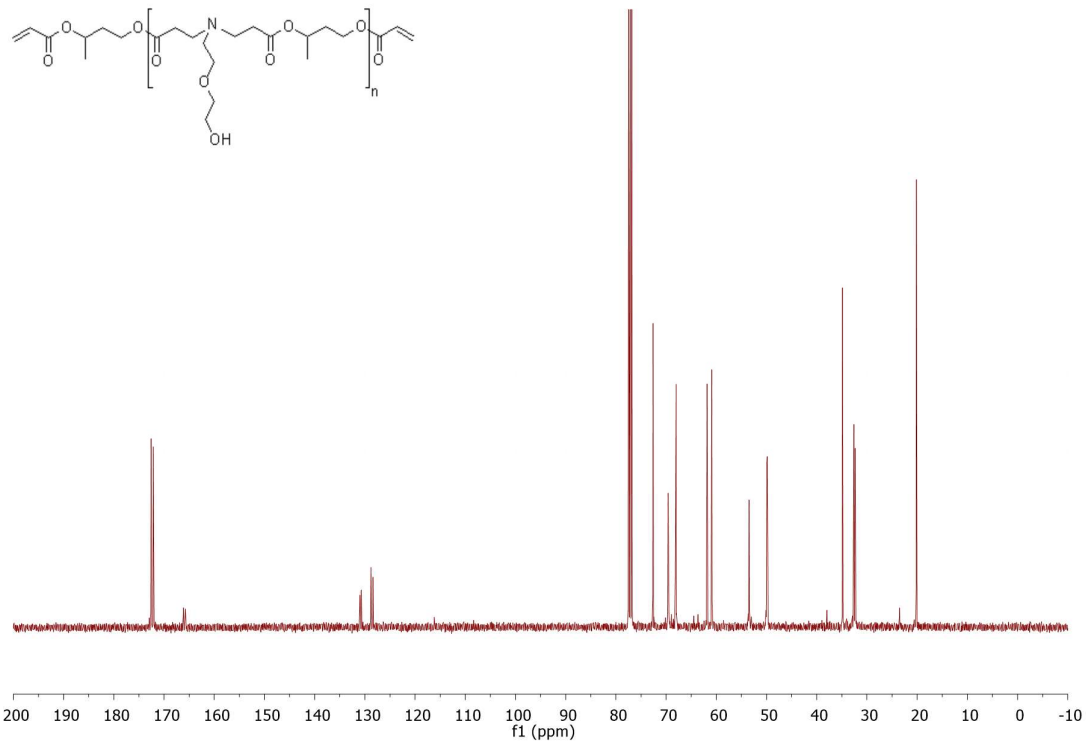

Figure S17. ^{13}C NMR spectrum ($CDCl_3$, 100 MHz) of PBAE *A1*.

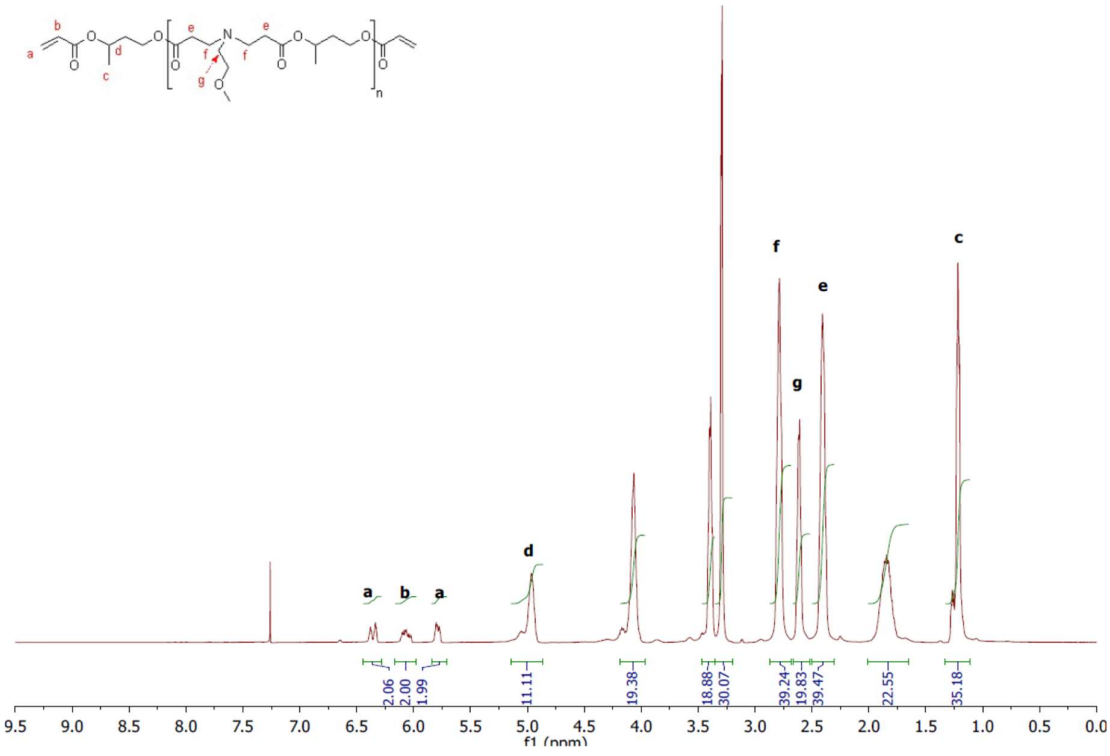

Figure S18. ^{1}H NMR spectrum ($CDCl_3$, 400 MHz) of PBAE *A2* (n=10).

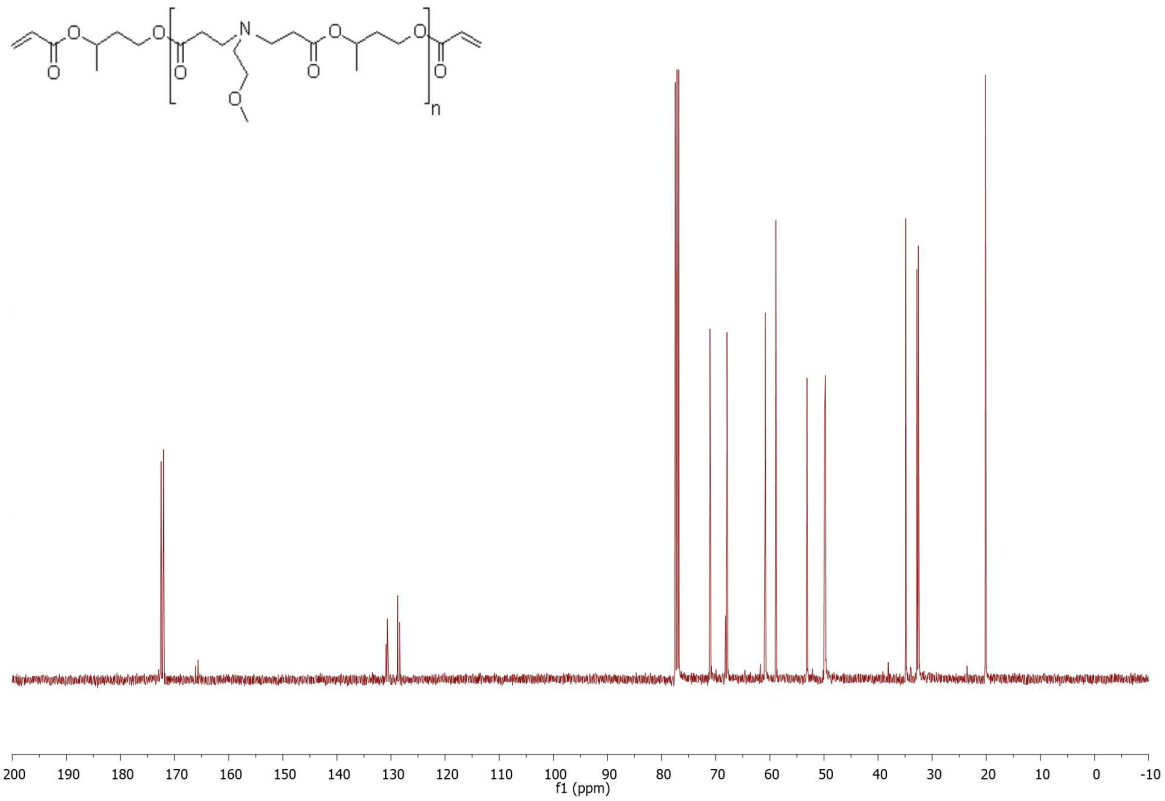

Figure S19. ^{13}C NMR spectrum ($CDCl_3$, 100 MHz) of PBAE *A2*.

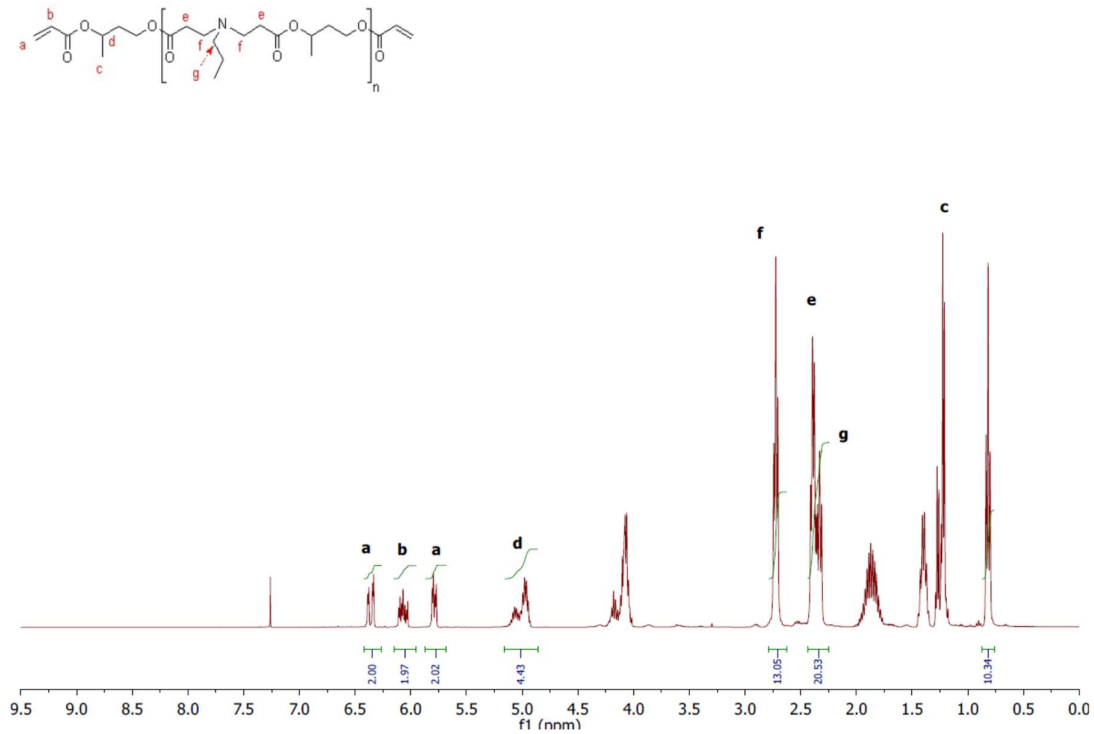

Figure S20. ^{1}H NMR spectrum ($CDCl_3$, 400 MHz) of PBAE *A3* (n=3).

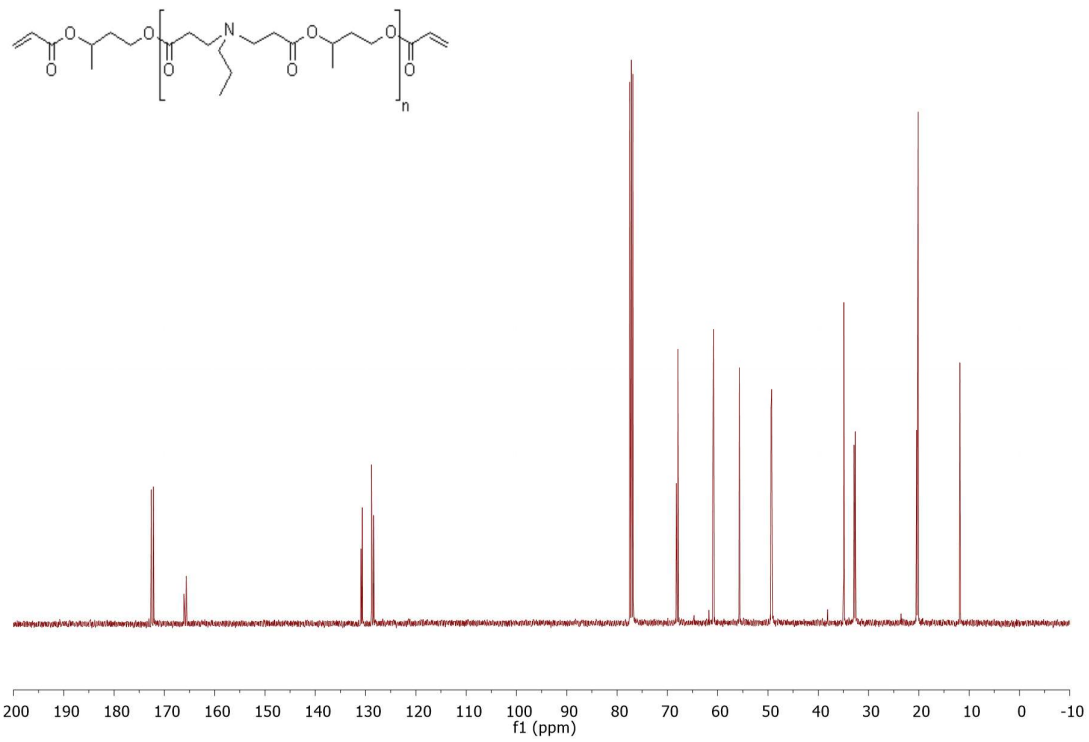

Figure S21. ^{13}C NMR spectrum ($CDCl_3$, 100 MHz) of PBAE *A3*.

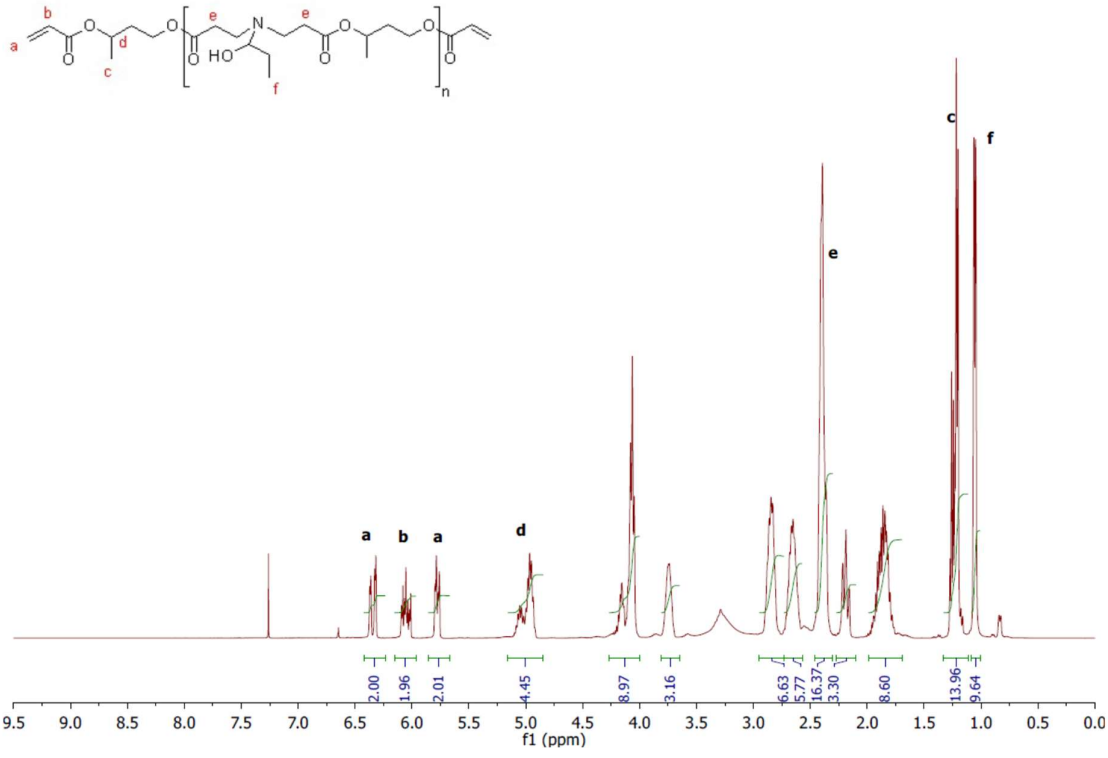

Figure S22. ^{1}H NMR spectrum ($CDCl_3$, 400 MHz) of PBAE *A5* (n=3).

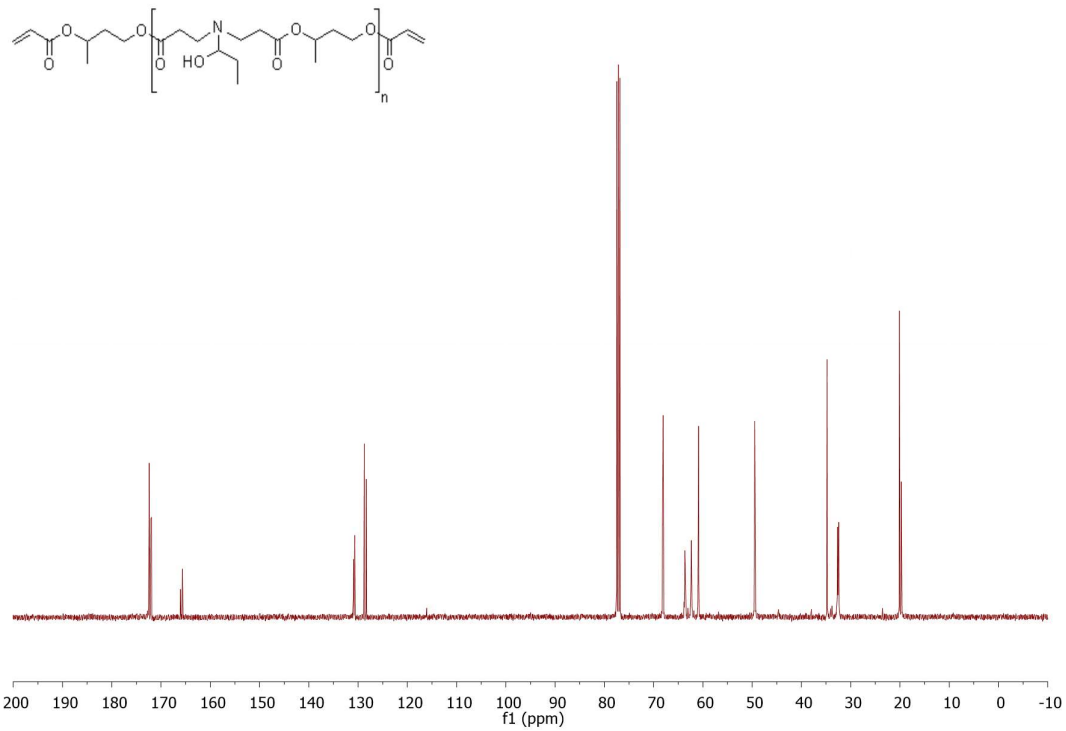

Figure S23. ^{13}C NMR spectrum ($CDCl_3$, 100 MHz) of PBAE *A5*.

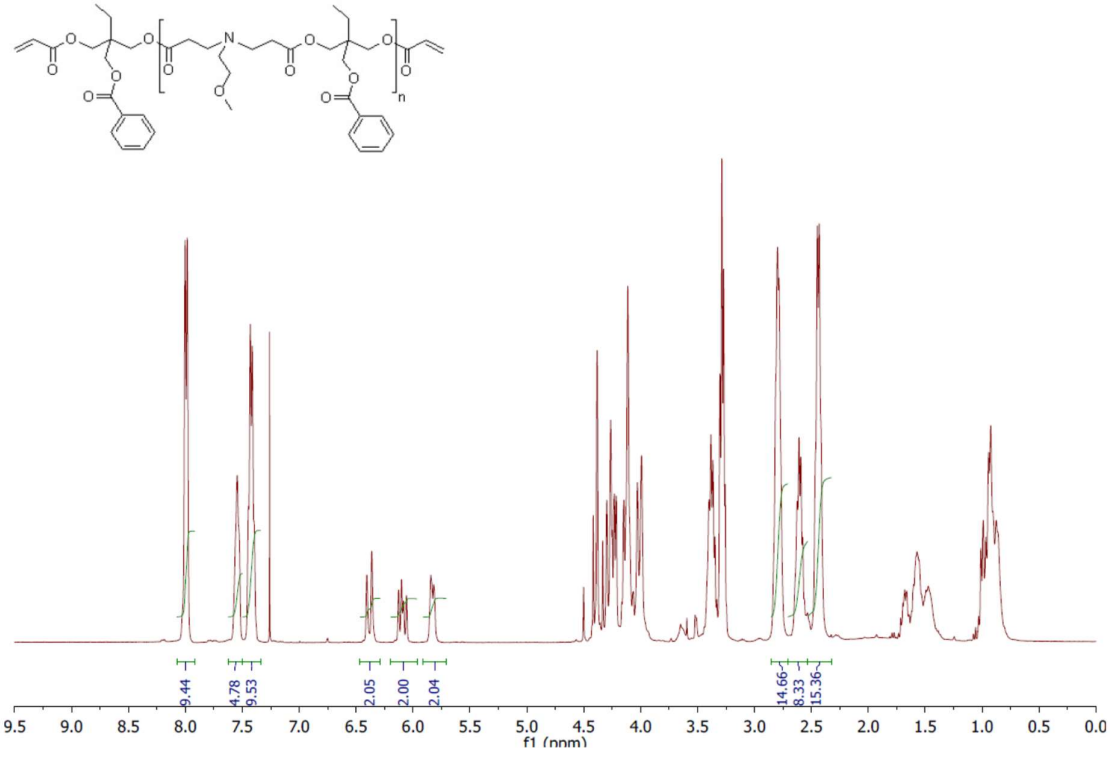

Figure S24. ^{1}H NMR spectrum ($CDCl_3$, 400 MHz) of PBAE *B2* (n=4).

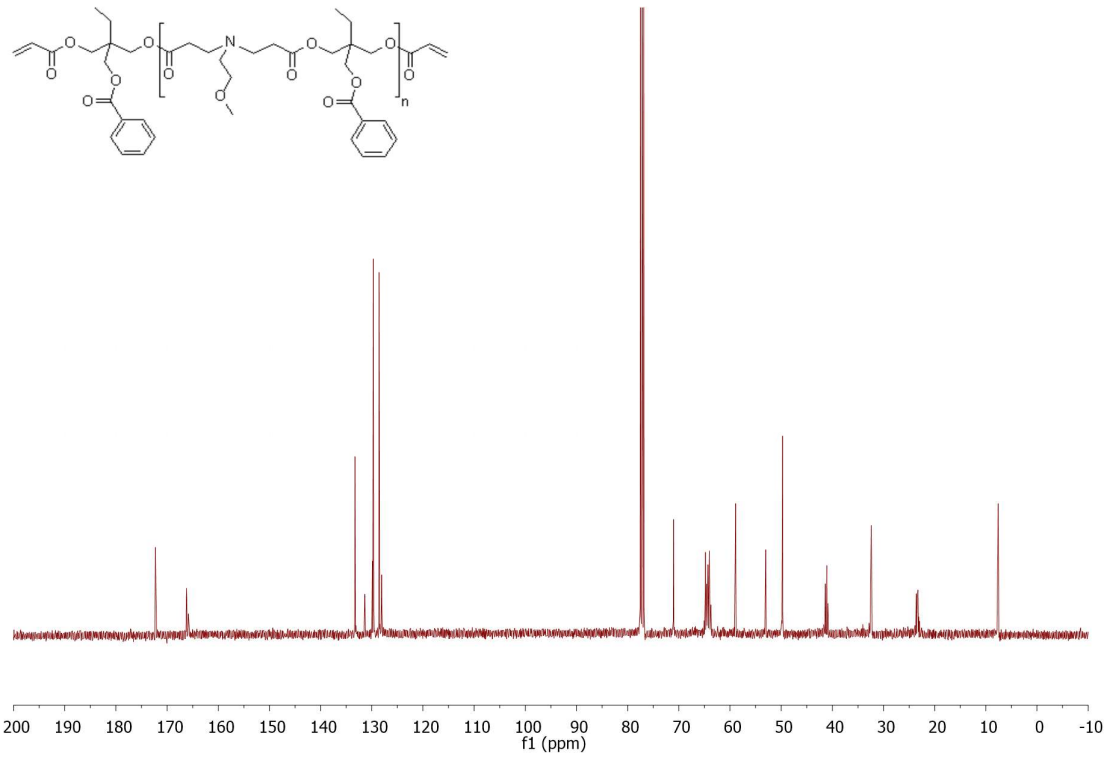

Figure S25. ^{13}C NMR spectrum ($CDCl_3$, 100 MHz) of PBAE *B2*.

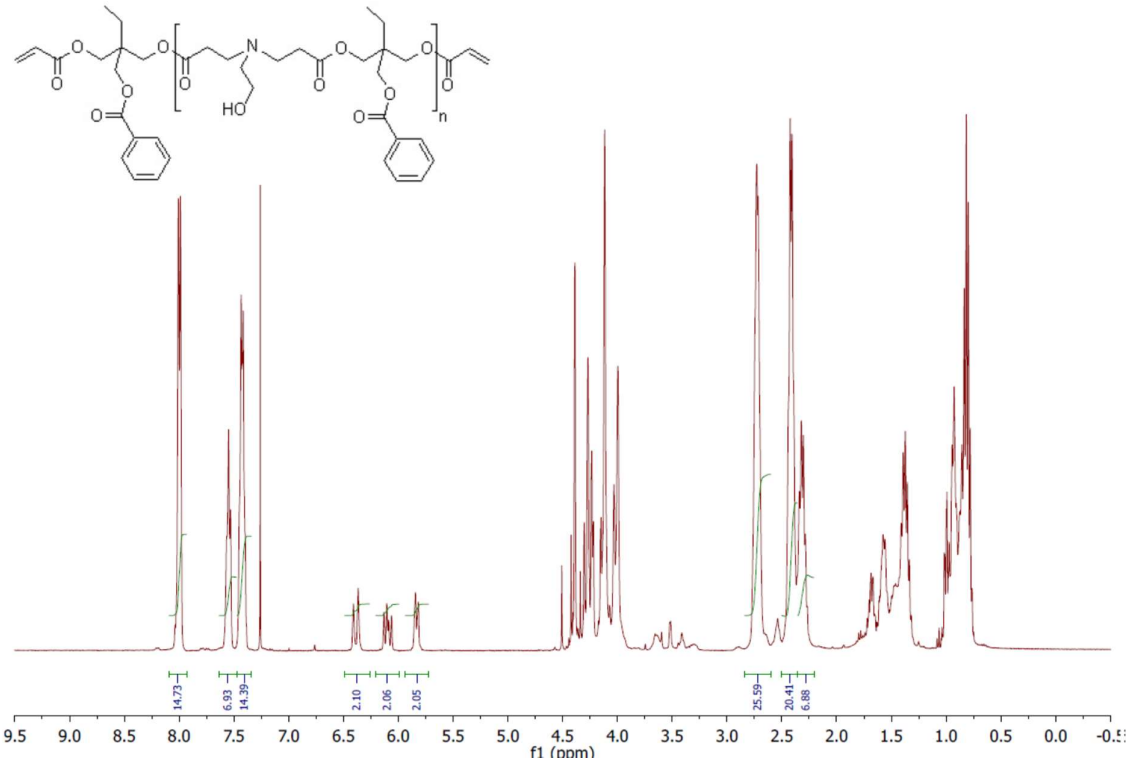

Figure S26. ^{1}H NMR spectrum ($CDCl_3$, 400 MHz) of PBAE *B3* (n=6).

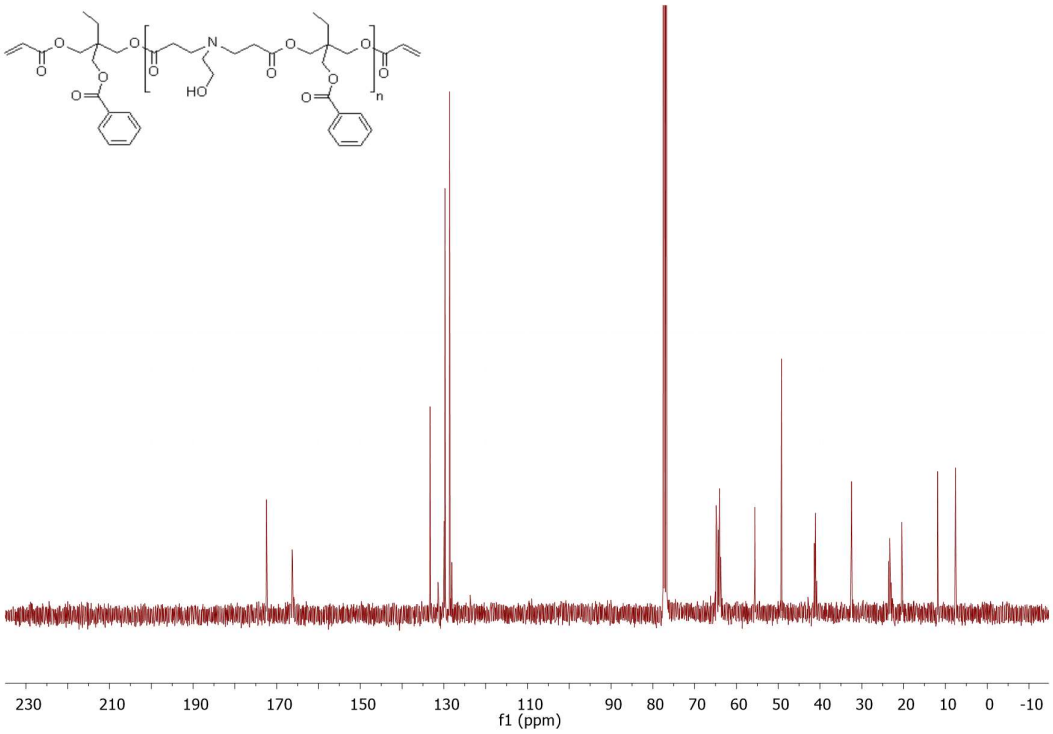

Figure S27. ^{13}C NMR spectrum ($CDCl_3$, 100 MHz) of PBAE *B3*.

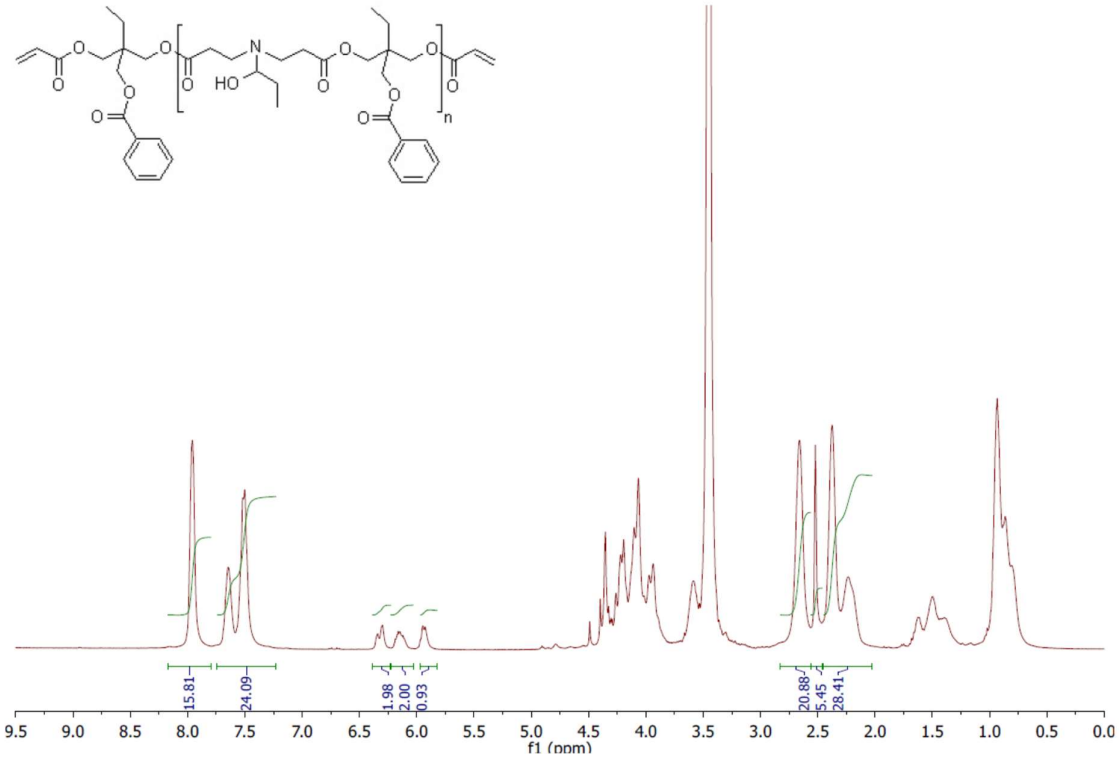

Figure S28. ^{1}H NMR spectrum (DMSO-d_6, 400 MHz) of PBAE *B5*.

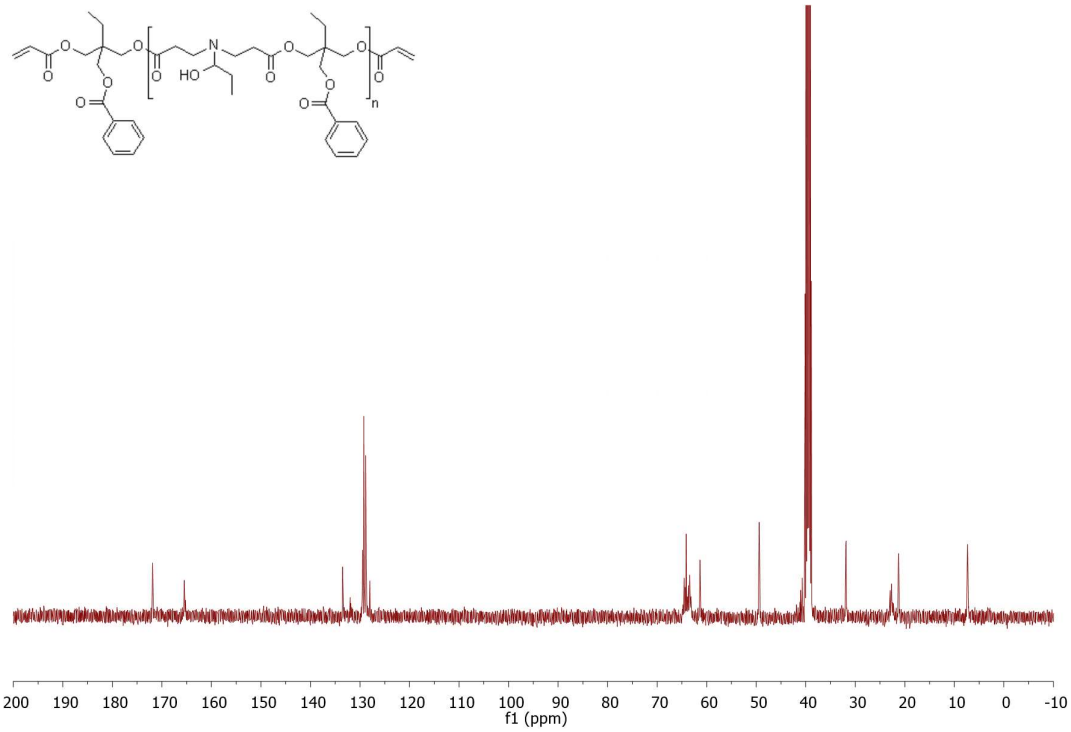

Figure S29. ^{13}C NMR spectrum (DMSO-d_6, 100 MHz) of PBAE *B5*.

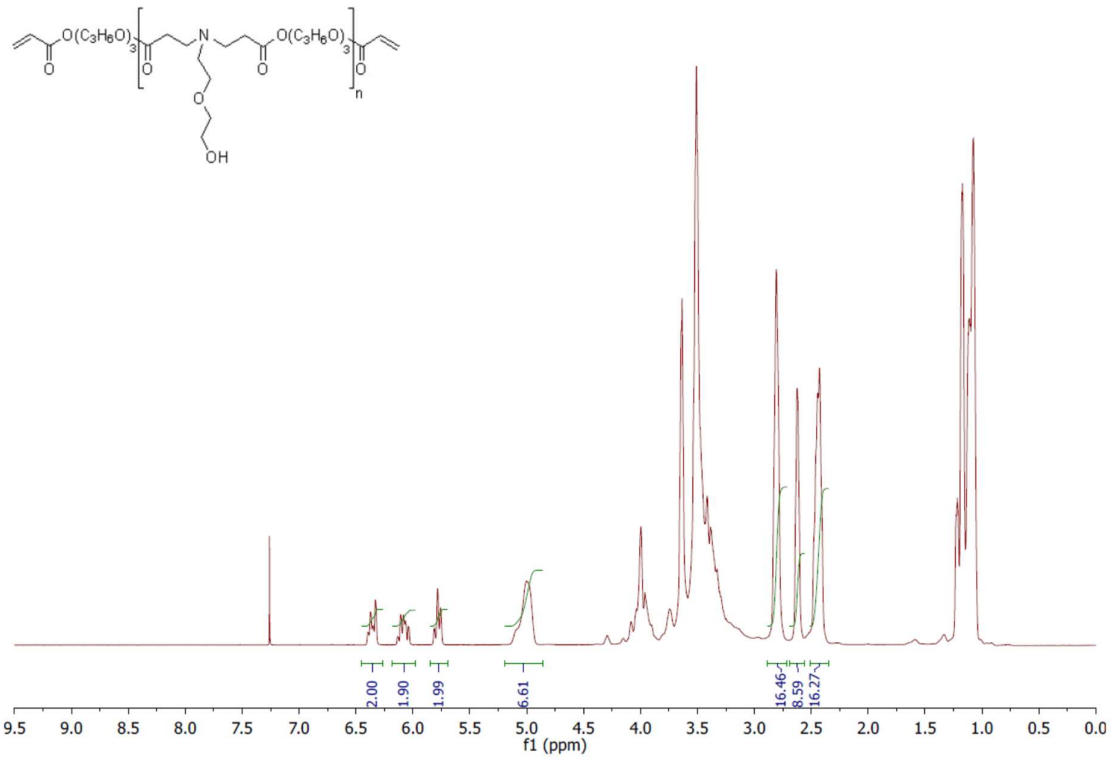

Figure S30. ^{1}H NMR spectrum ($CDCl_3$, 400 MHz) of PBAE *C1* (n=4).

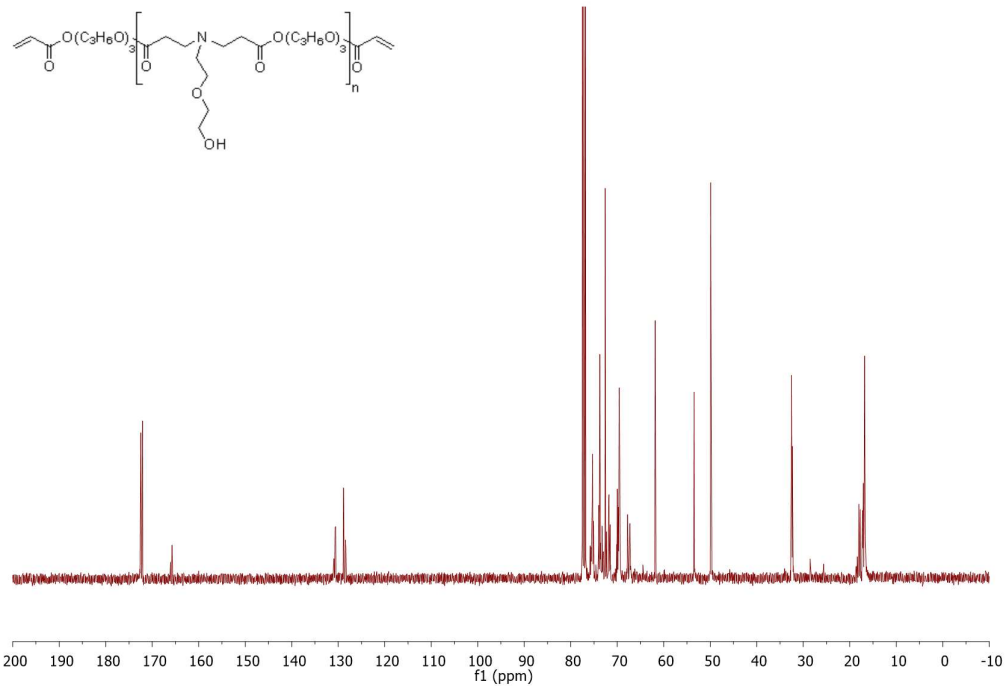

Figure S31. ^{13}C NMR spectrum ($CDCl_3$, 100 MHz) of PBAE *C1*.

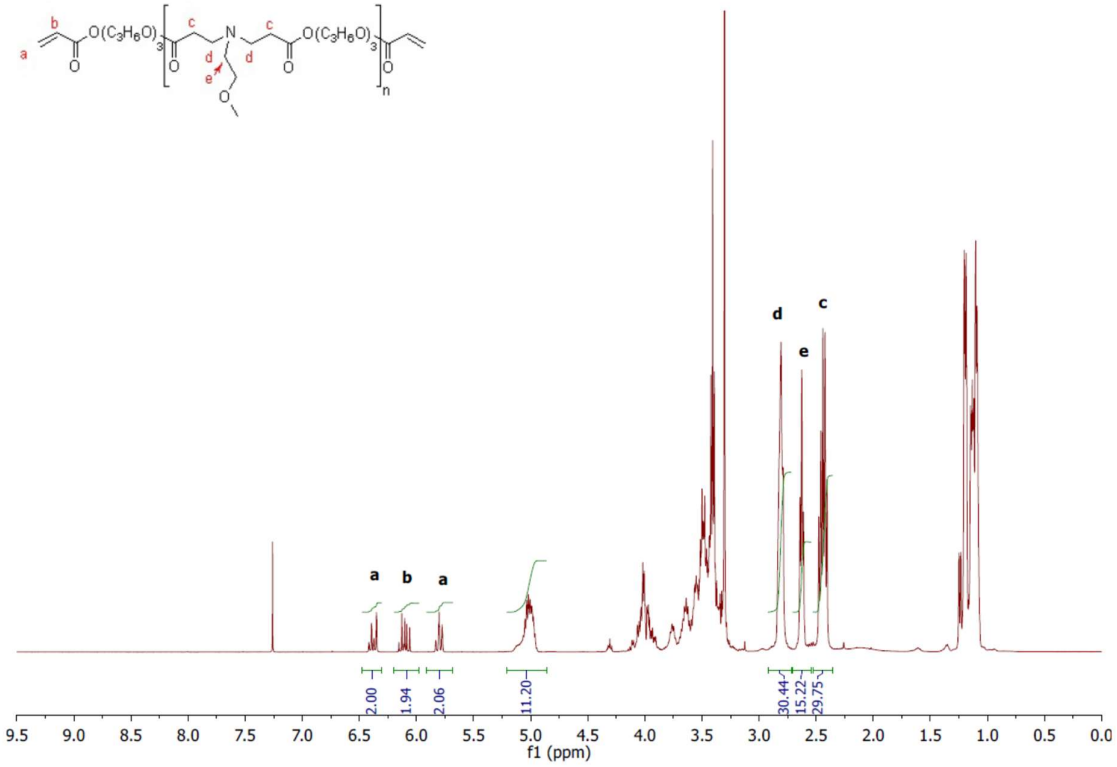

Figure S32. ^{1}H NMR spectrum ($CDCl_3$, 400 MHz) of PBAE *C2* (n=8-9).

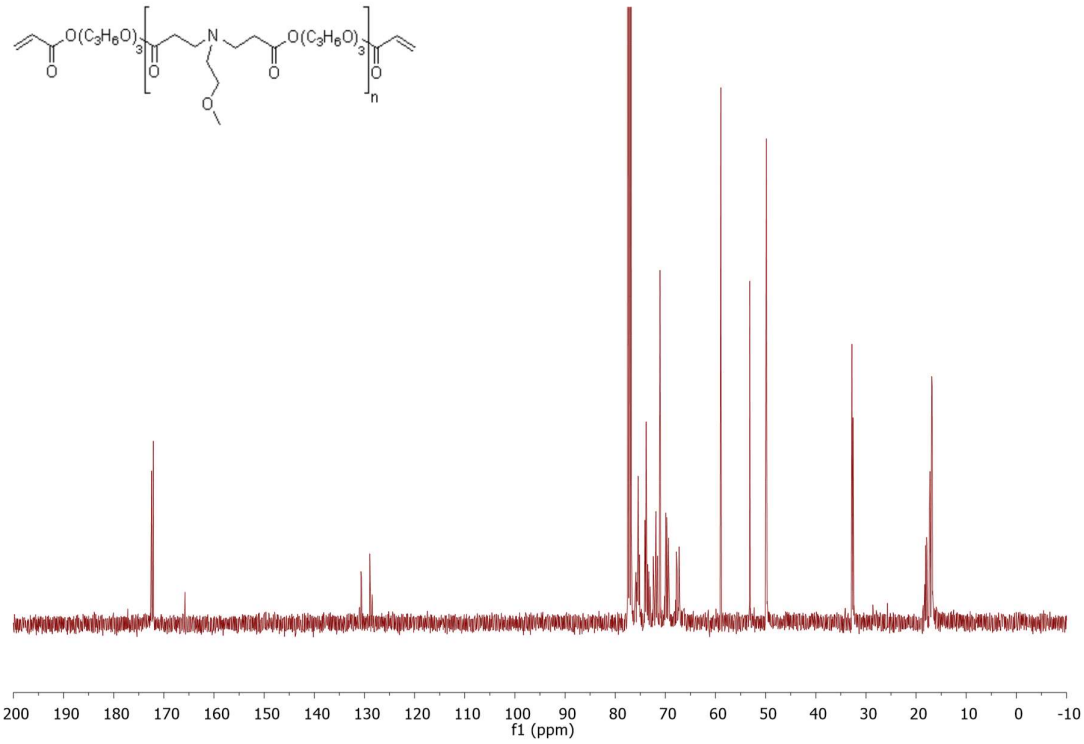

Figure S33. ^{13}C NMR spectrum ($CDCl_3$, 100 MHz) of PBAE *C2*.

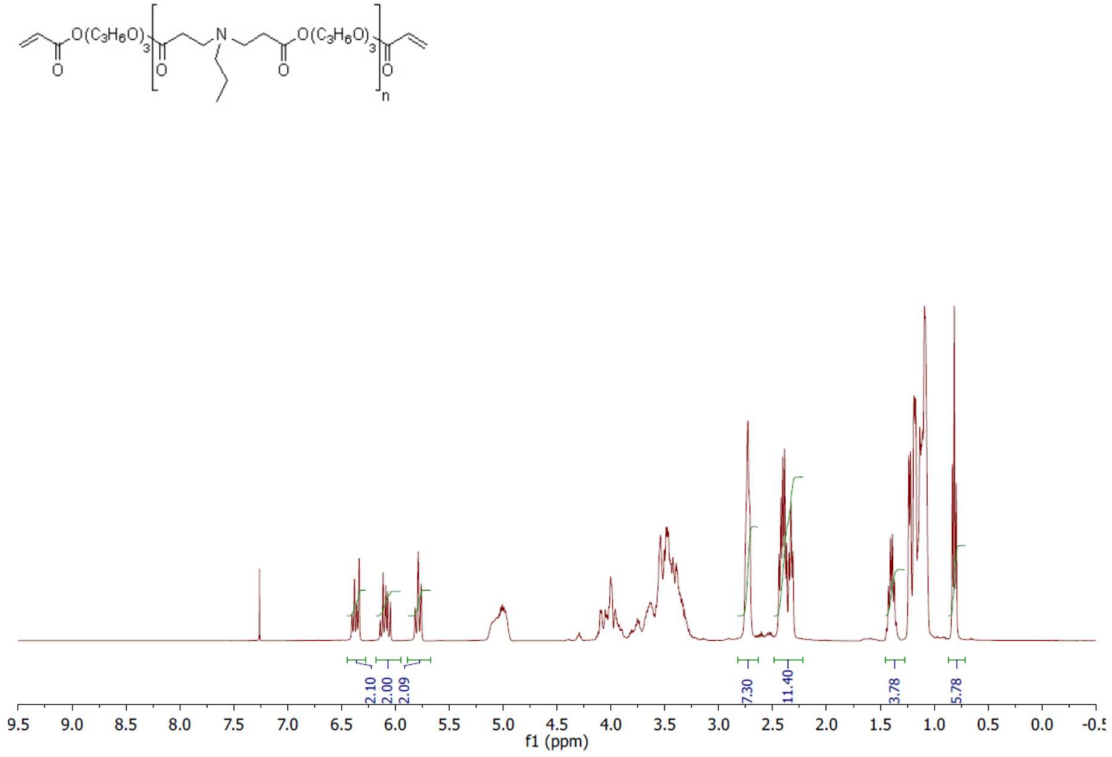

Figure S34. ^{1}H NMR spectrum ($CDCl_3$, 400 MHz) of PBAE *C3* (n=2).

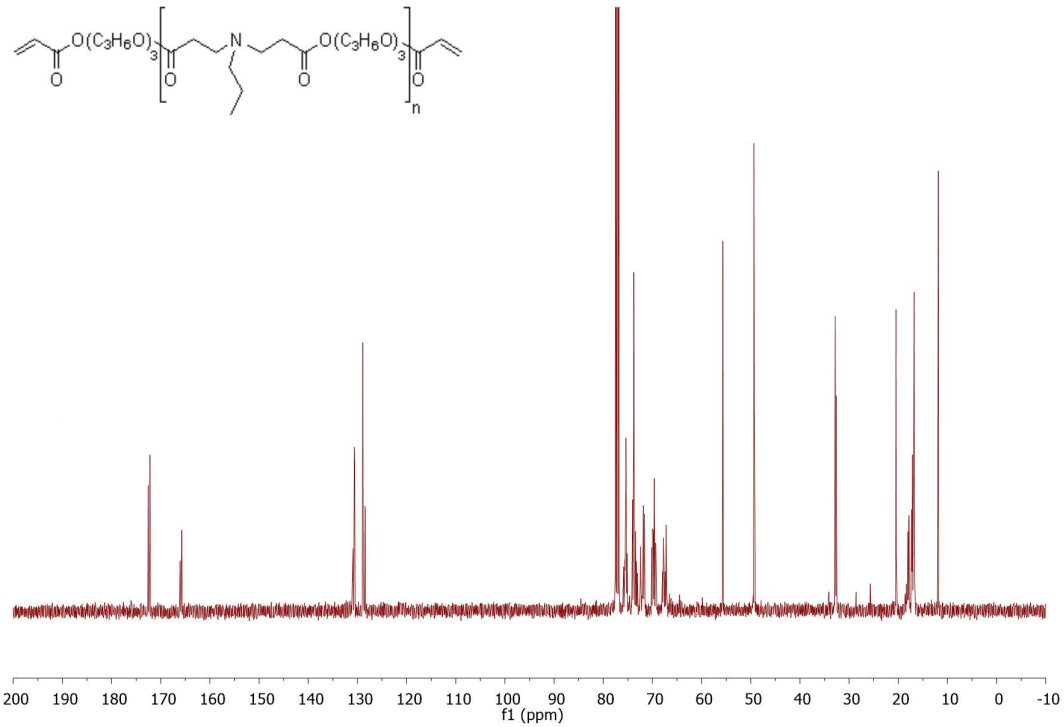

Figure S35. ^{13}C NMR spectrum ($CDCl_3$, 100 MHz) of PBAE *C3*.

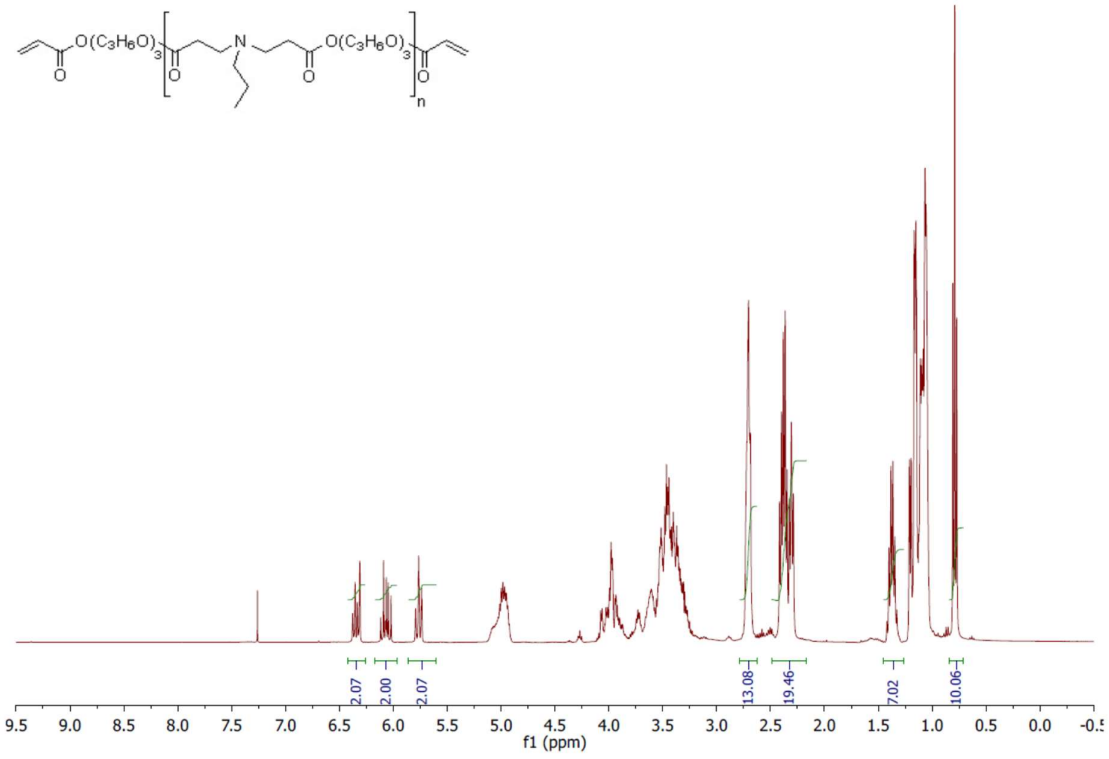

Figure S36. ^{1}H NMR spectrum ($CDCl_3$, 400 MHz) of PBAE *C3-15* (n=3).

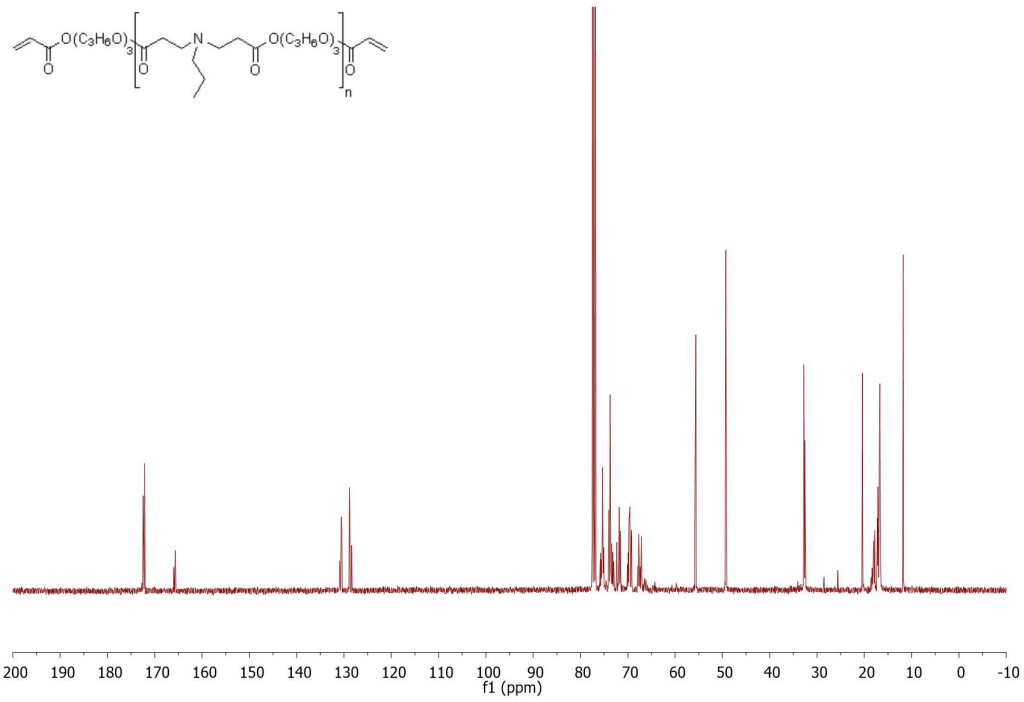

Figure S37. ^{13}C NMR spectrum ($CDCl_3$, 100 MHz) of PBAE *C3-15*.

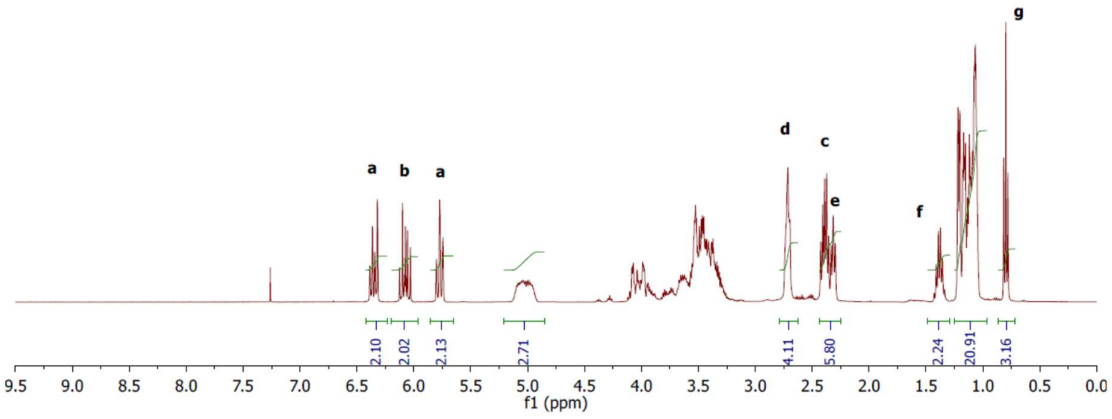

Figure S38. ^{1}H NMR spectrum ($CDCl_3$, 400 MHz) of PBAE *C3-2* (n=1).

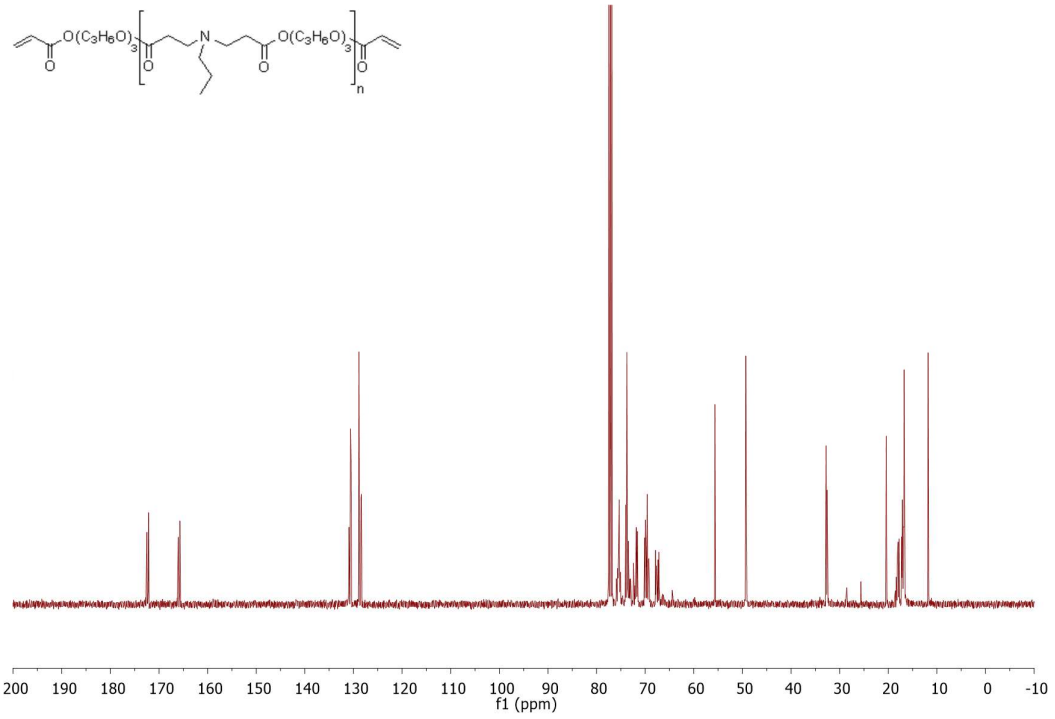

Figure S39. ^{13}C NMR spectrum ($CDCl_3$, 100 MHz) of PBAE *C3-2*.

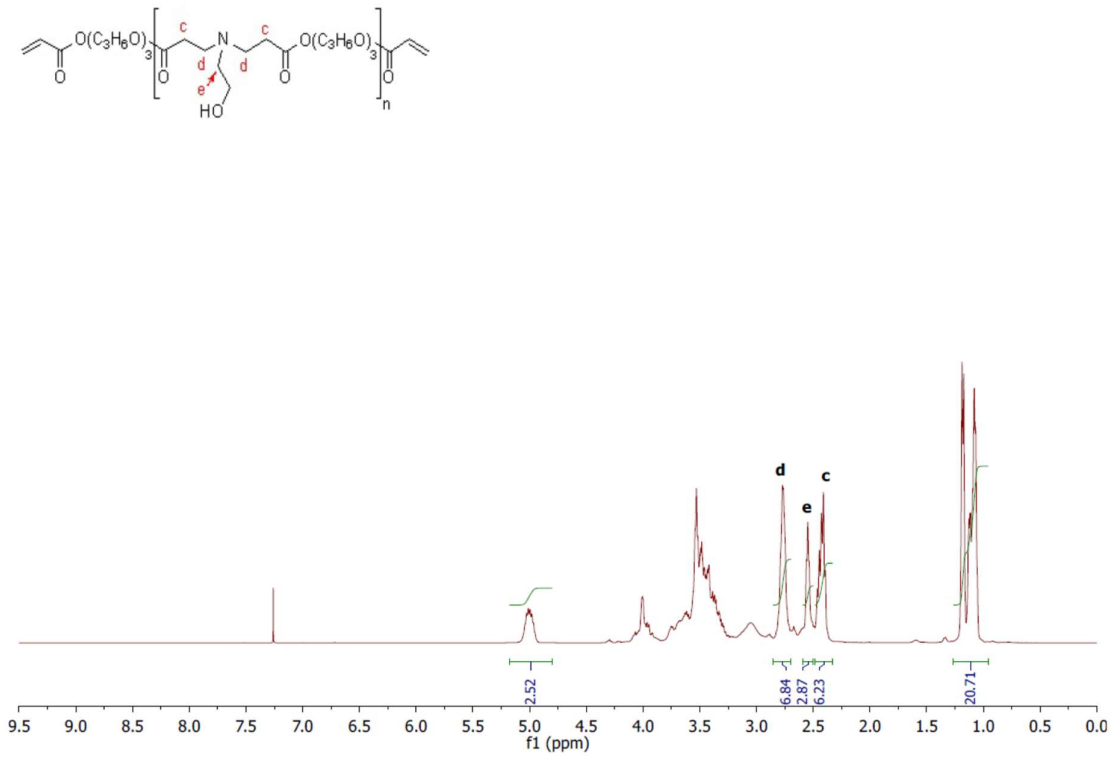

Figure S40. ^{1}H NMR spectrum ($CDCl_3$, 400 MHz) of PBAE *C4* (n=2).

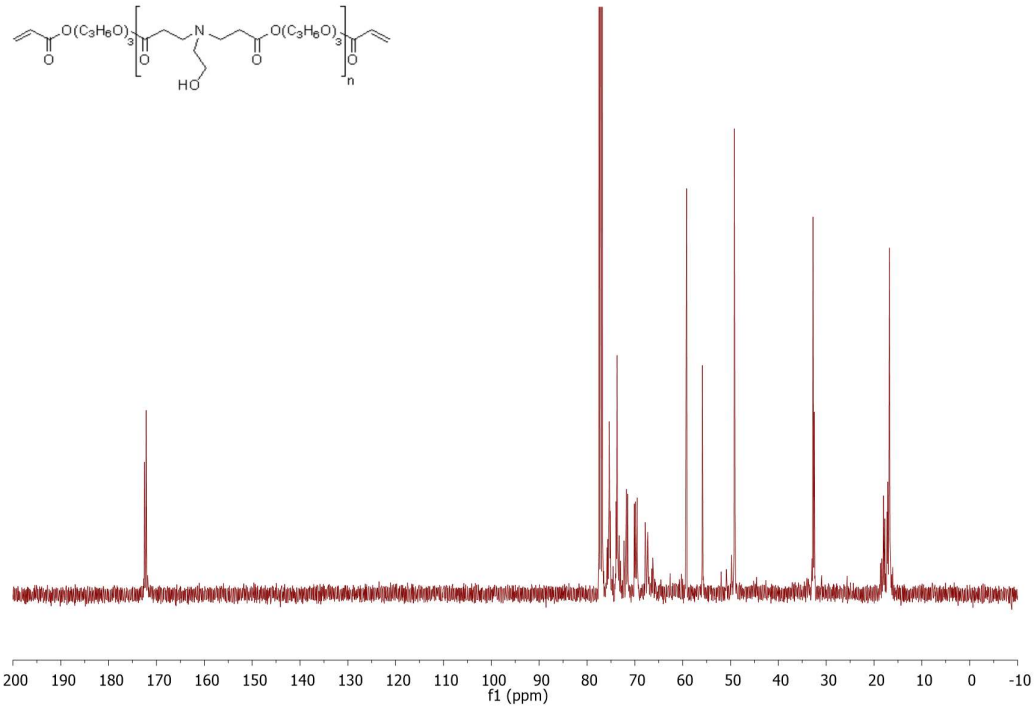

Figure S41. ^{13}C NMR spectrum ($CDCl_3$, 100 MHz) of PBAE *C4*.

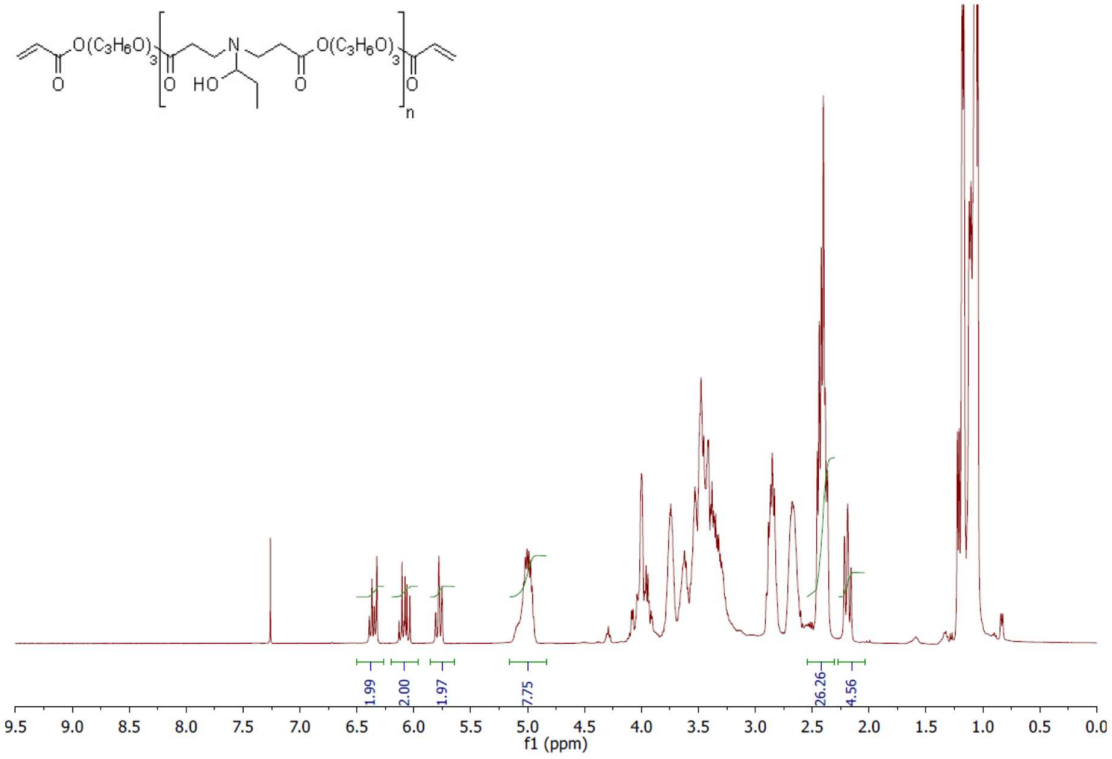

Figure S42. ^{1}H NMR spectrum ($CDCl_3$, 400 MHz) of PBAE *C5* (n=4-5).

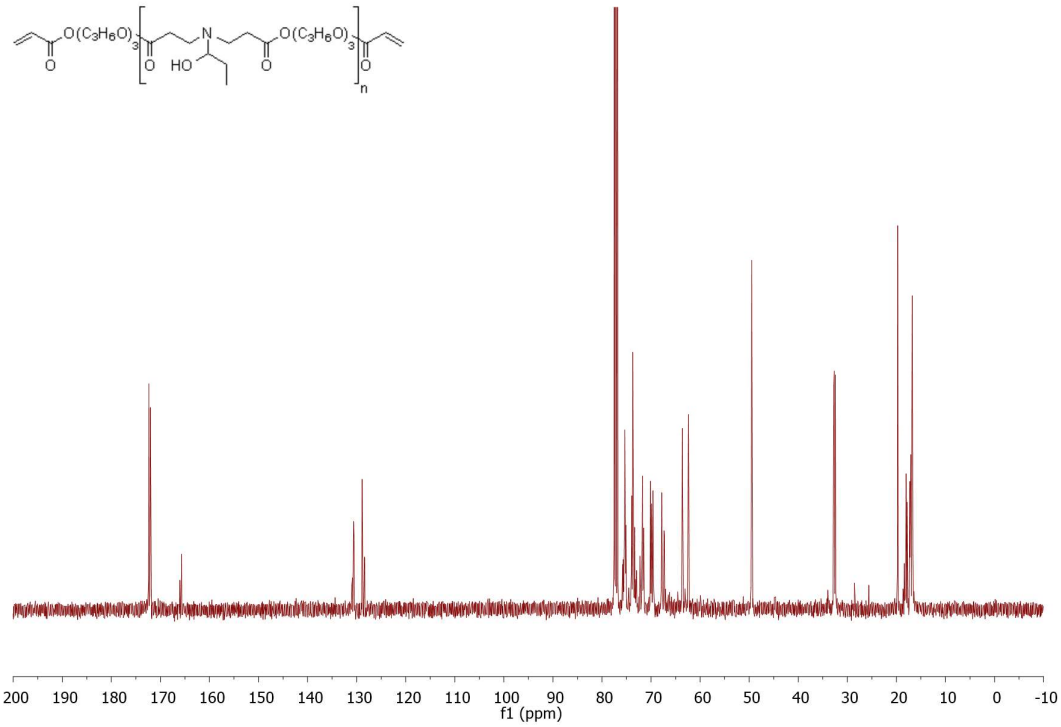

Figure S43. ^{13}C NMR spectrum ($CDCl_3$, 100 MHz) of PBAE *C5*.

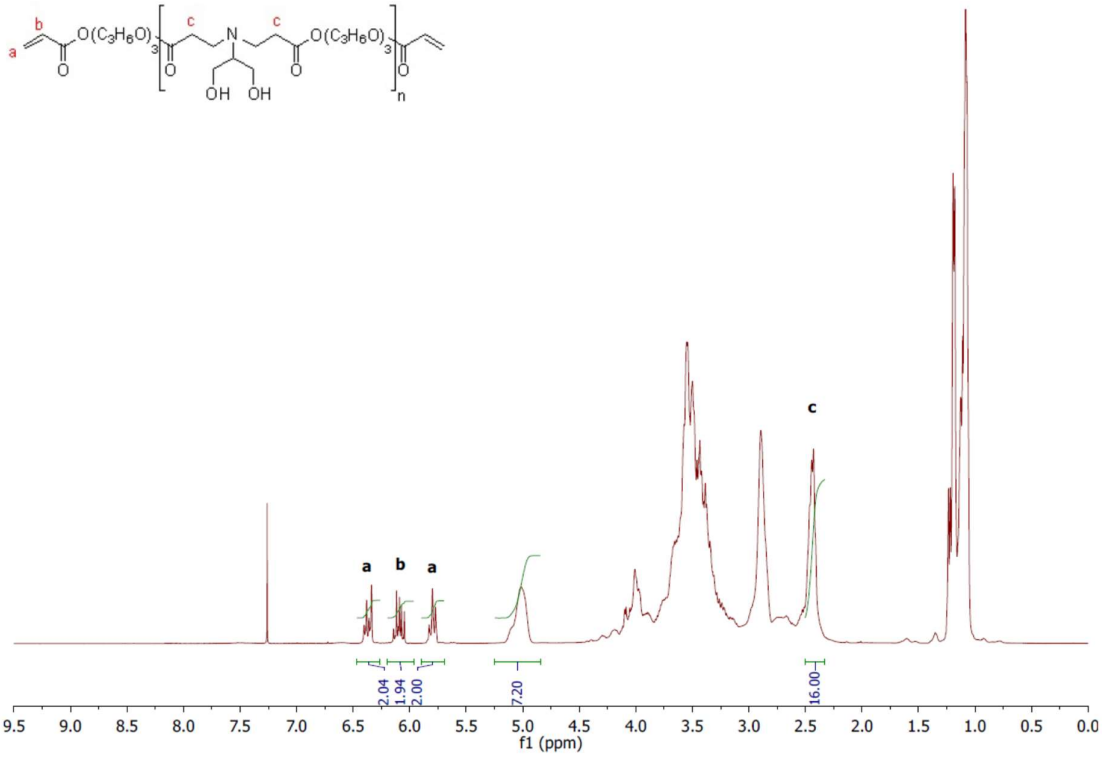

Figure S44. ^{1}H NMR spectrum ($CDCl_3$, 400 MHz) of PBAE *C6* (n=4).

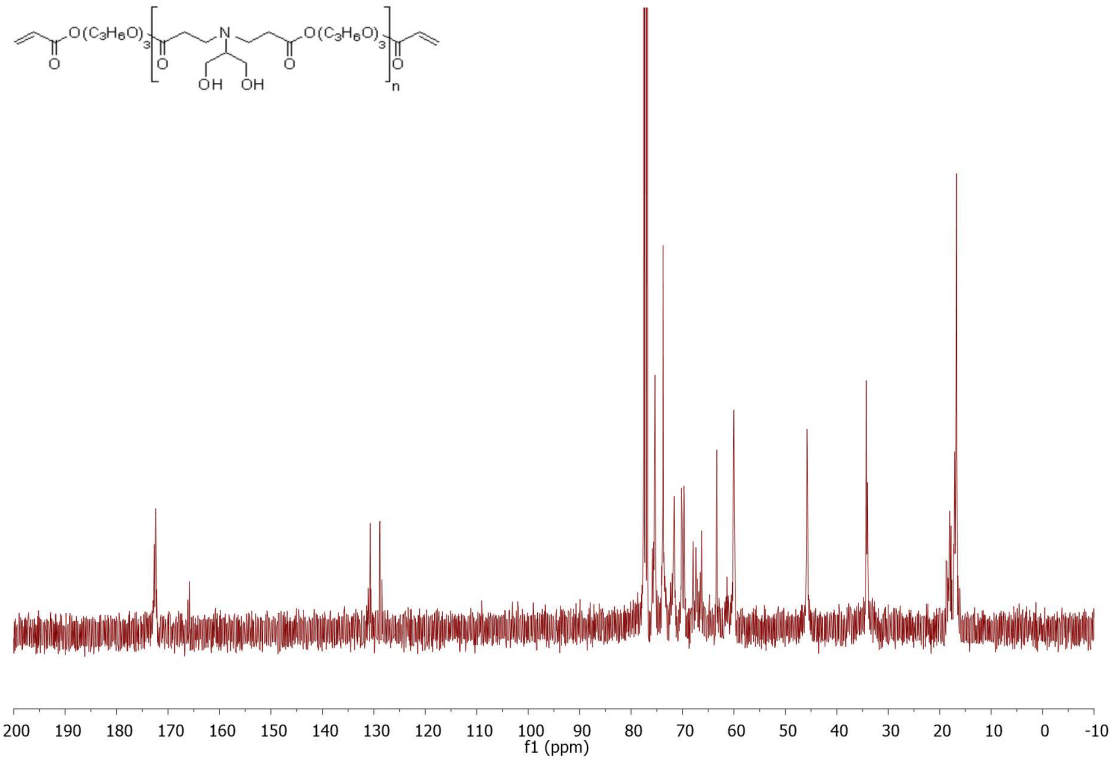

Figure S45. ^{13}C NMR spectrum ($CDCl_3$, 100 MHz) of PBAE *C6*.

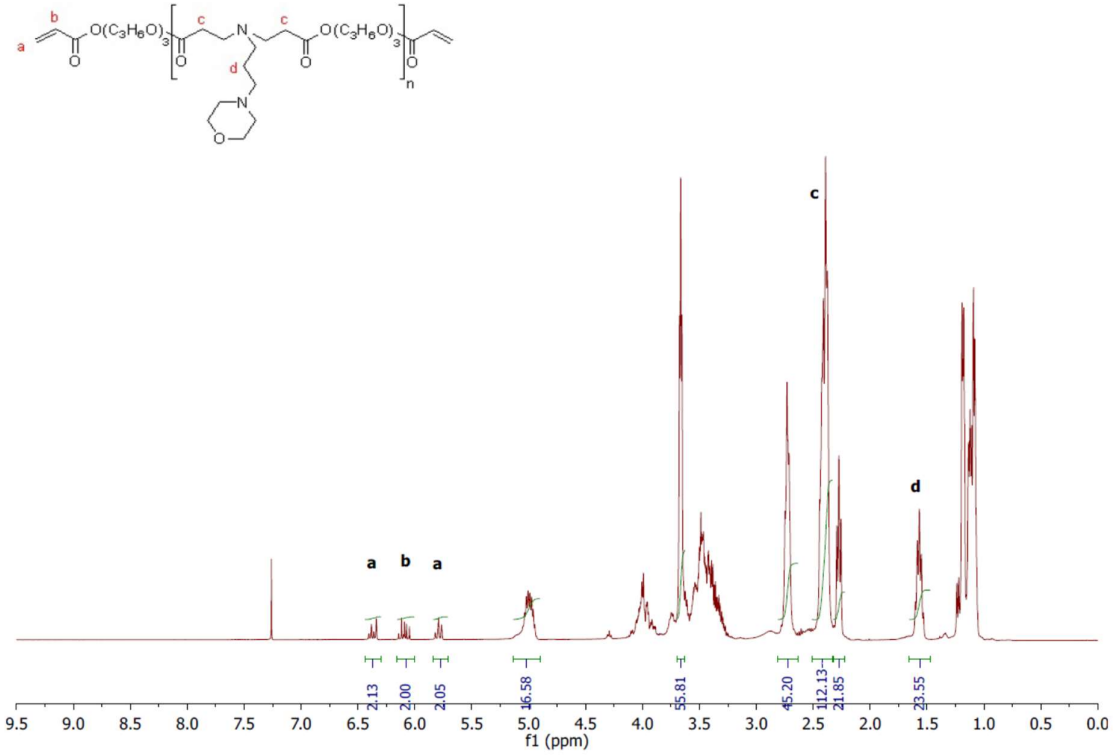

Figure S46. ^{1}H NMR spectrum ($CDCl_3$, 400 MHz) of PBAE *C7* (n=11).

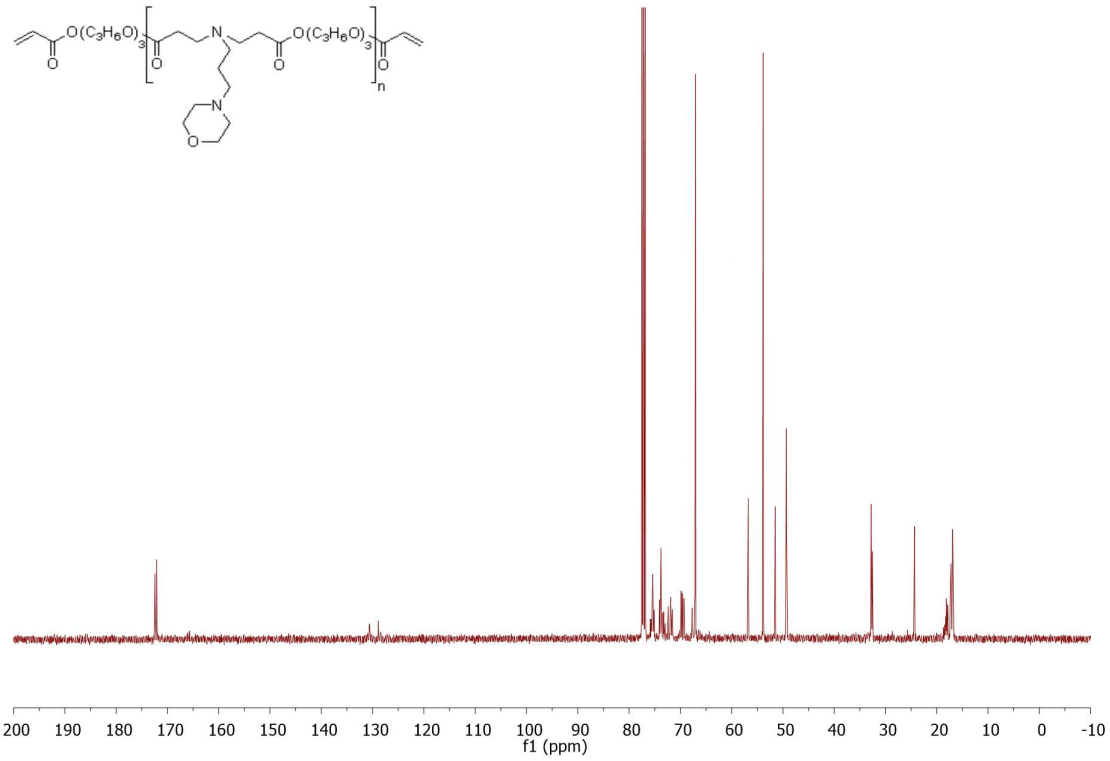

Figure S47. ^{13}C NMR spectrum ($CDCl_3$, 100 MHz) of PBAE *C7*.

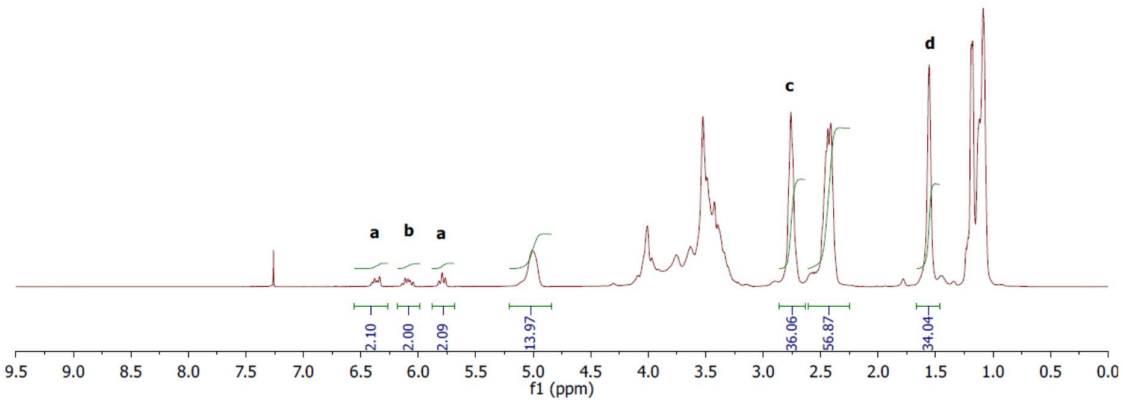

Figure S48. ^{1}H NMR spectrum ($CDCl_3$, 400 MHz) of PBAE *C8* (n=9).

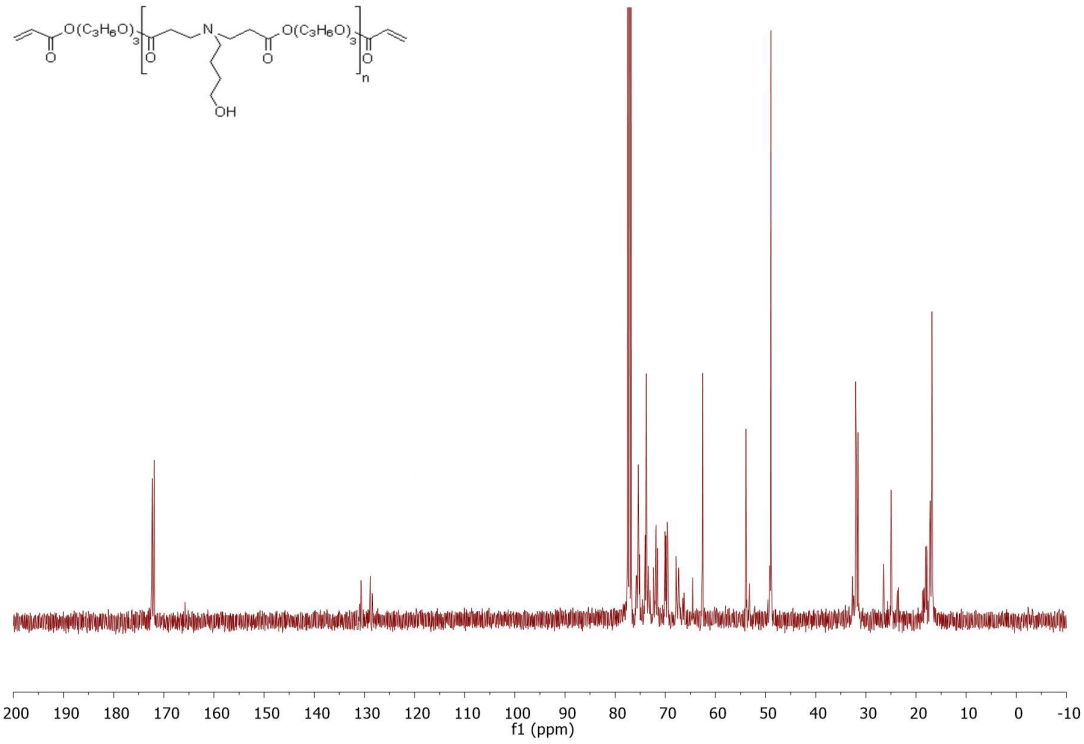

Figure S49. ^{13}C NMR spectrum ($CDCl_3$, 100 MHz) of PBAE *C8*.

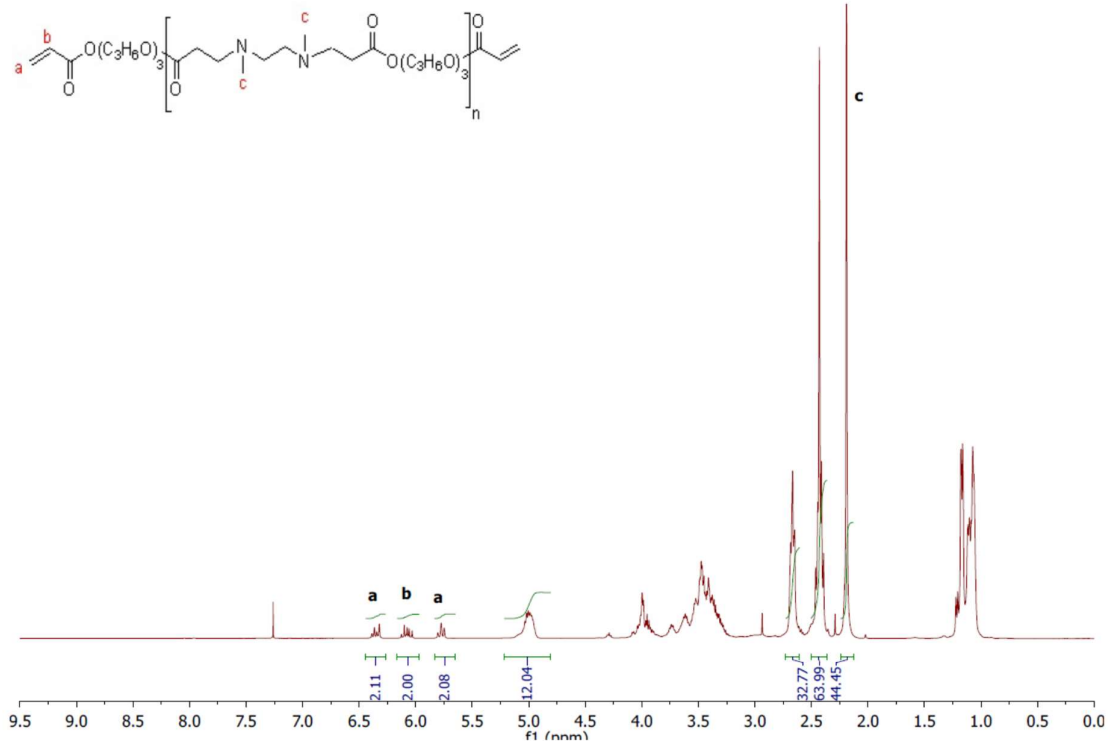

Figure S50. ^{1}H NMR spectrum ($CDCl_3$, 400 MHz) of PBAE *C9* (n=7-8).

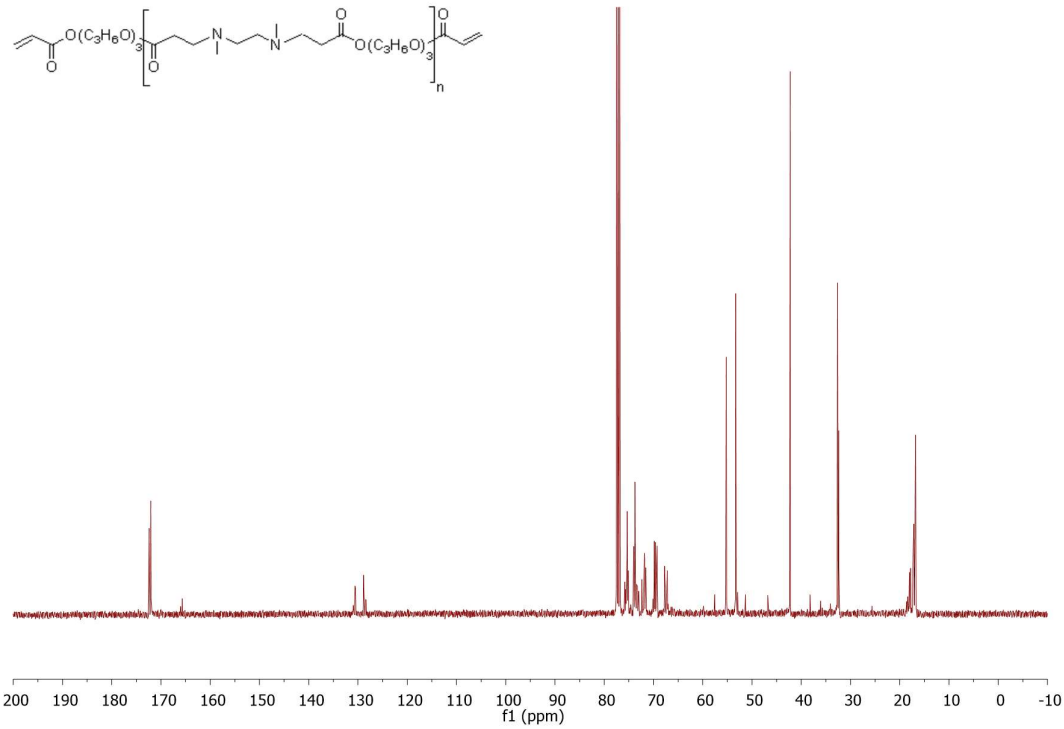

Figure S51. ^{13}C NMR spectrum ($CDCl_3$, 100 MHz) of PBAE *C9*.

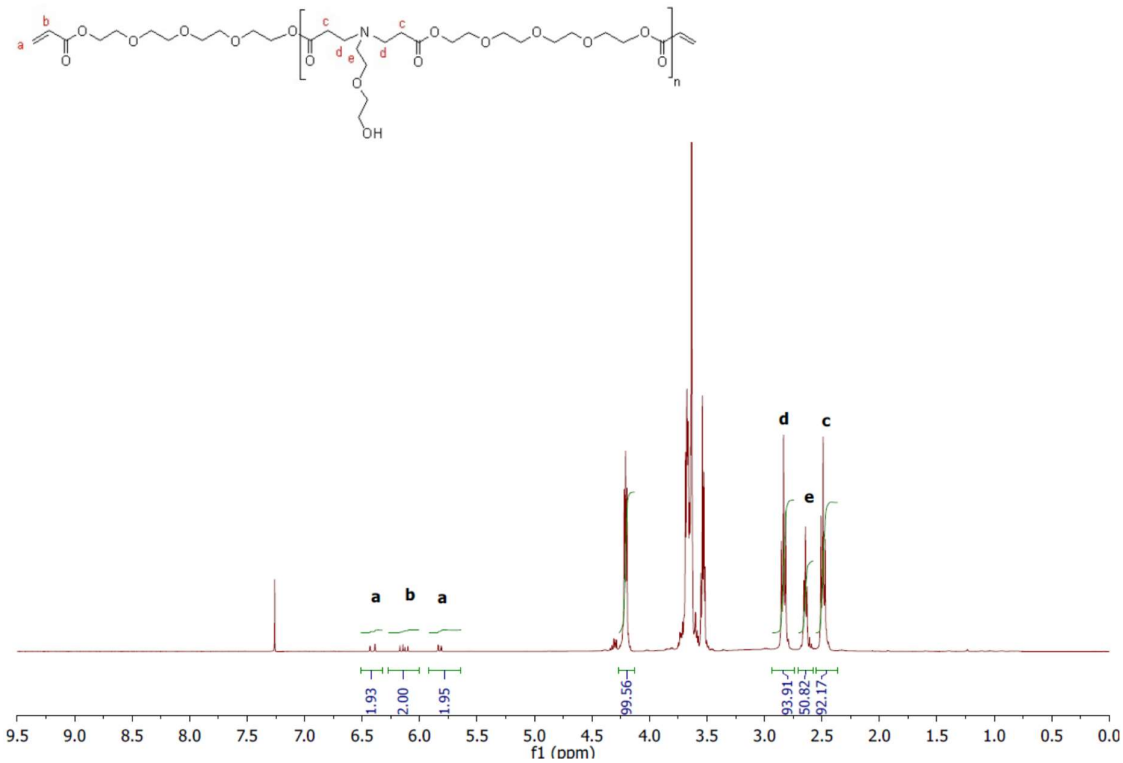

Figure S52. ^{1}H NMR spectrum ($CDCl_3$, 400 MHz) of PBAE *D1* (n= 25).

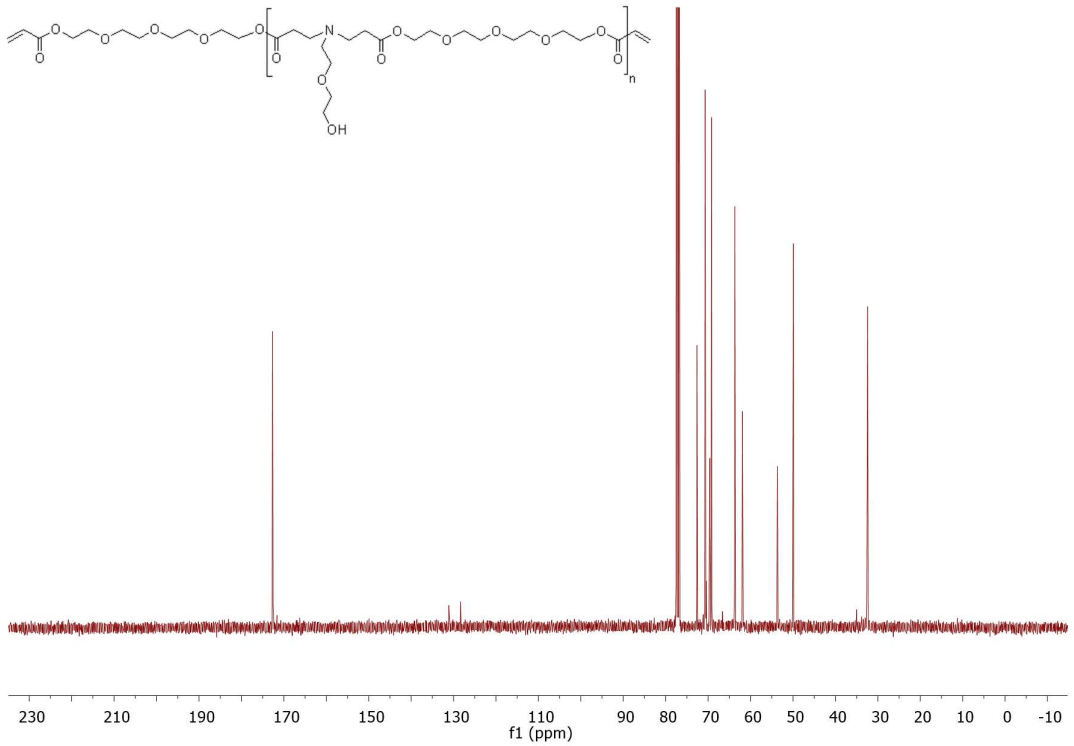

Figure S53. ^{13}C NMR spectrum ($CDCl_3$, 100 MHz) of PBAE *D1*.

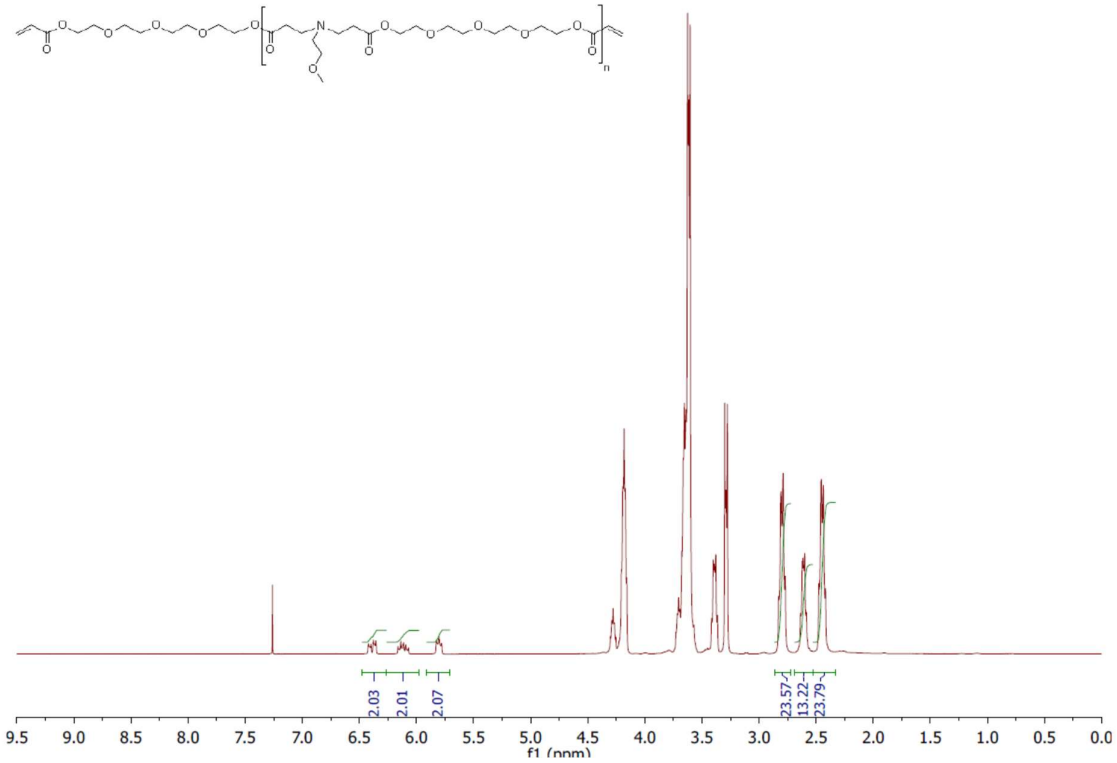

Figure S54. ^{1}H NMR spectrum ($CDCl_3$, 400 MHz) of PBAE *D2* (n=6).

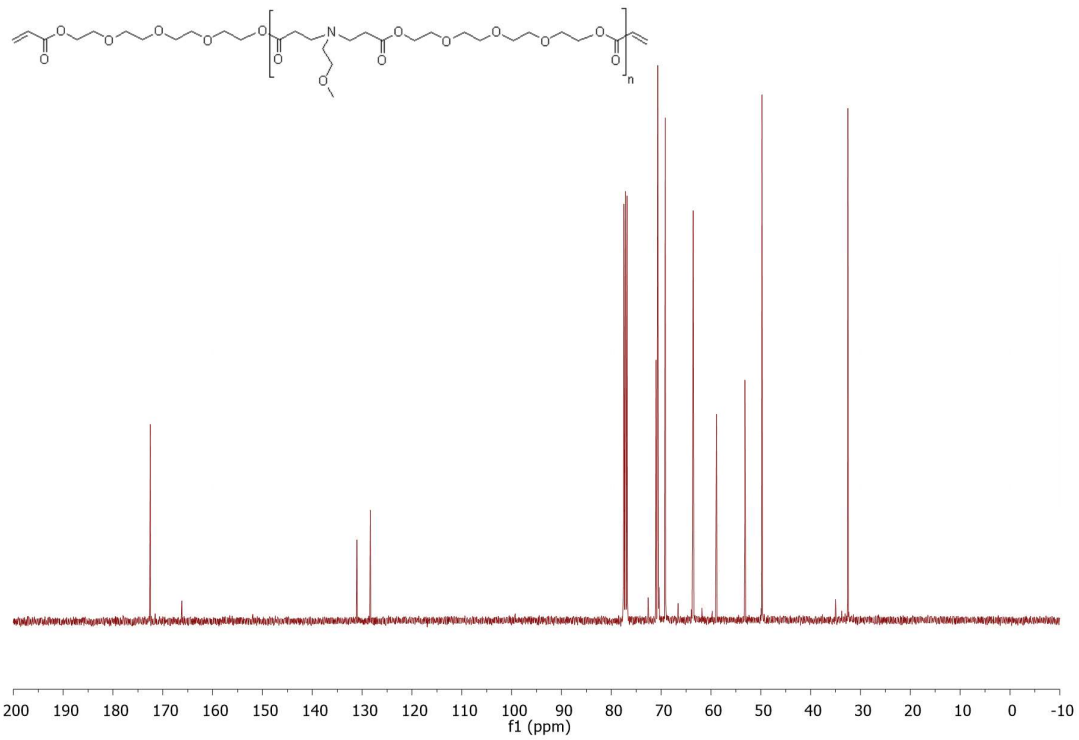

Figure S55. ^{13}C NMR spectrum ($CDCl_3$, 100 MHz) of PBAE *D2*.

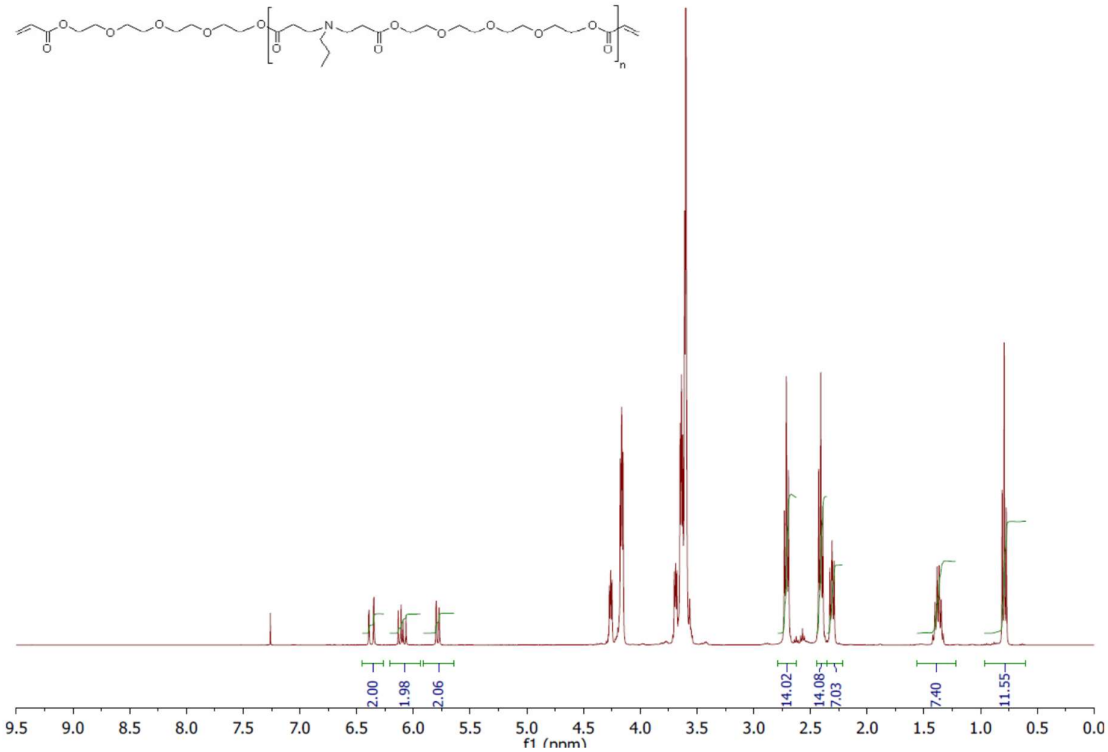

Figure S56. ^{1}H NMR spectrum ($CDCl_3$, 400 MHz) of PBAE *D3* (n=4).

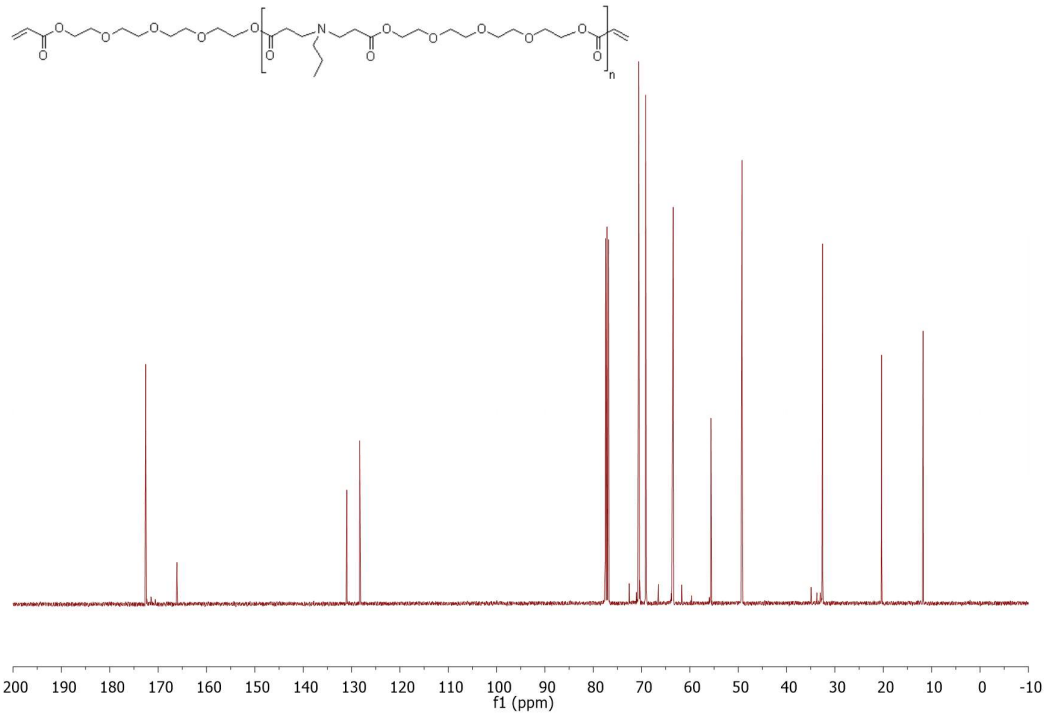

Figure S57. ^{13}C NMR spectrum ($CDCl_3$, 100 MHz) of PBAE *D3*.

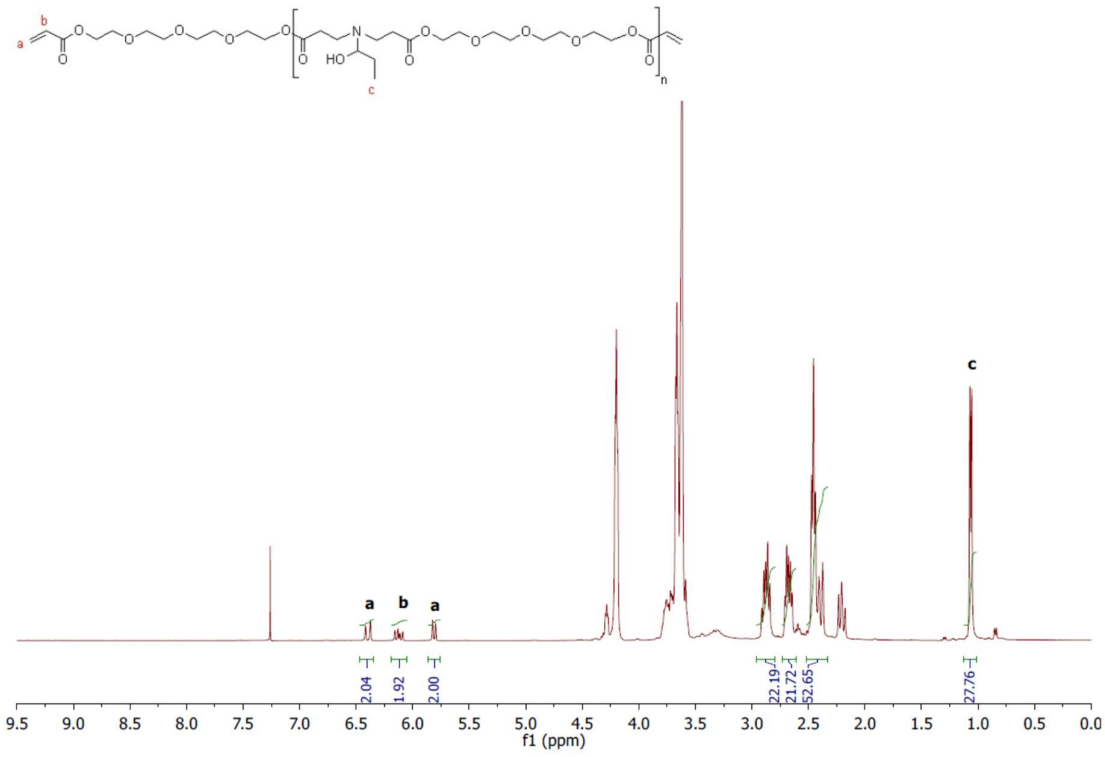

Figure S58. ^{1}H NMR spectrum ($CDCl_3$, 400 MHz) of PBAE *D5* (n=9).

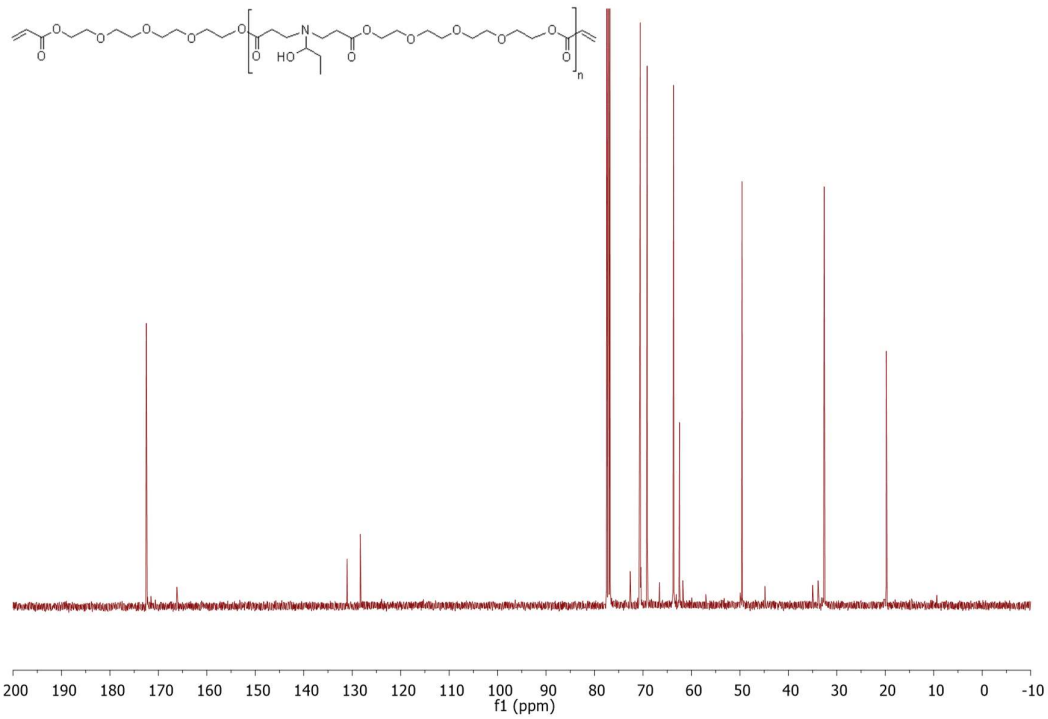

Figure S59. ^{13}C NMR spectrum ($CDCl_3$, 100 MHz) of PBAE *D5*.

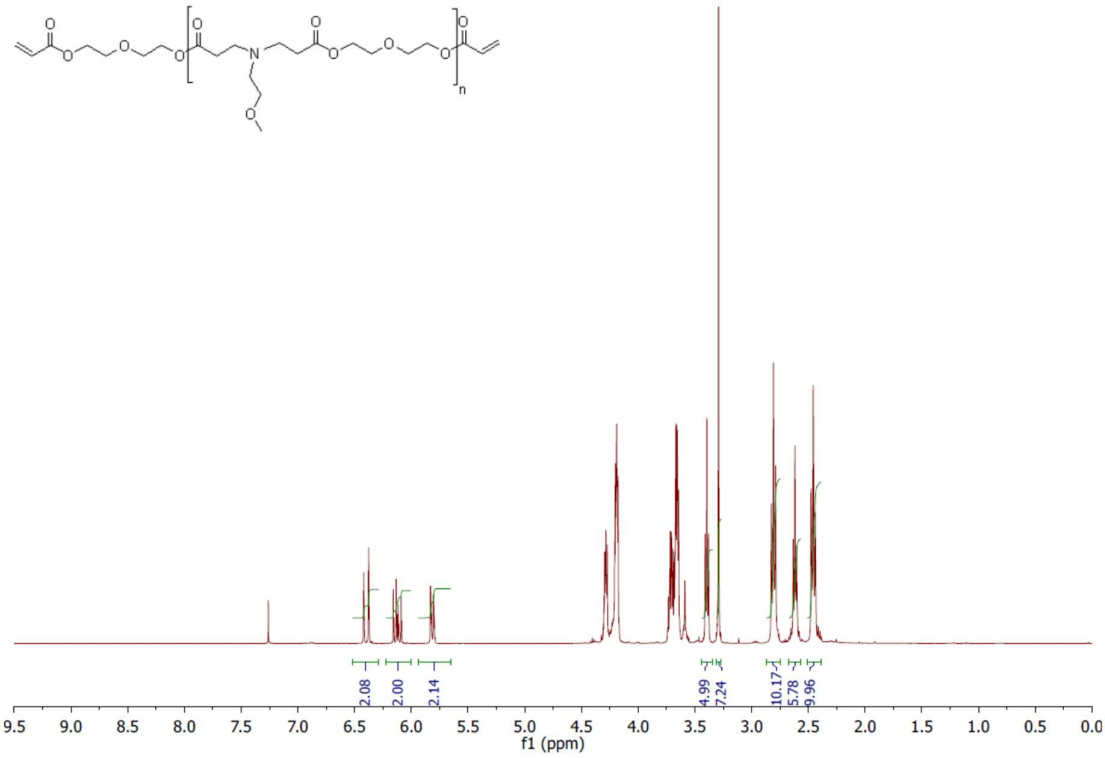

Figure S60. ^{1}H NMR spectrum ($CDCl_3$, 400 MHz) of PBAE *E2* (n=2).

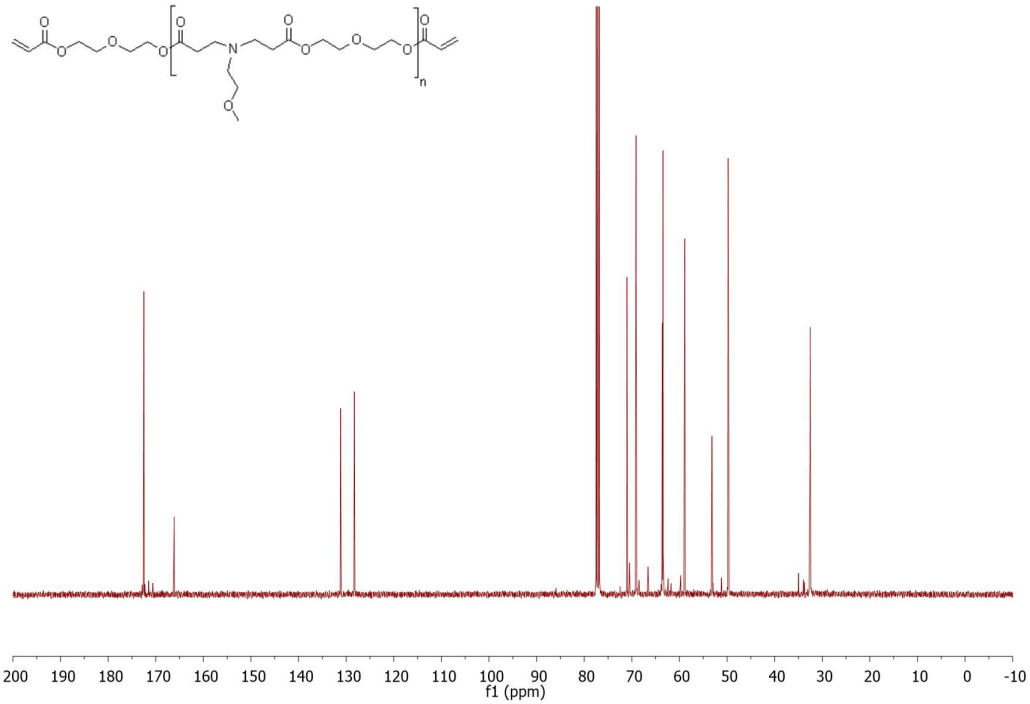

Figure S61. ^{13}C NMR spectrum ($CDCl_3$, 100 MHz) of PBAE *E2*.

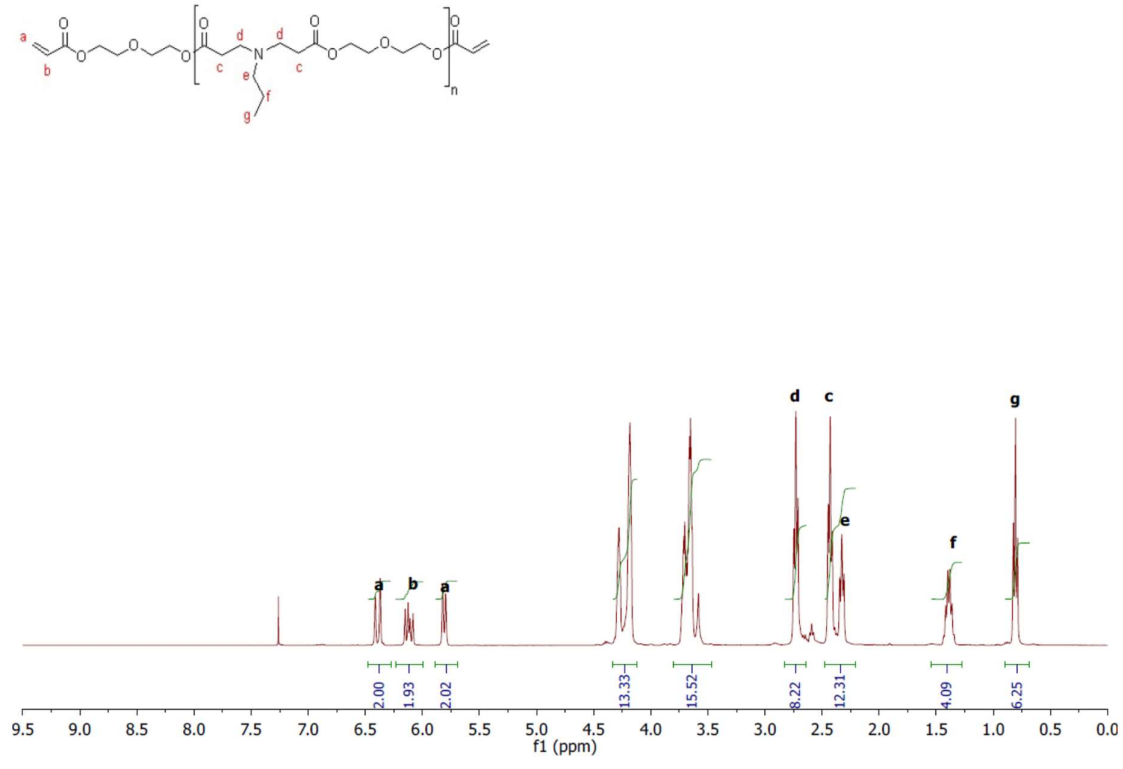

Figure S62. ^{1}H NMR spectrum ($CDCl_3$, 400 MHz) of PBAE *E3* (n=2).

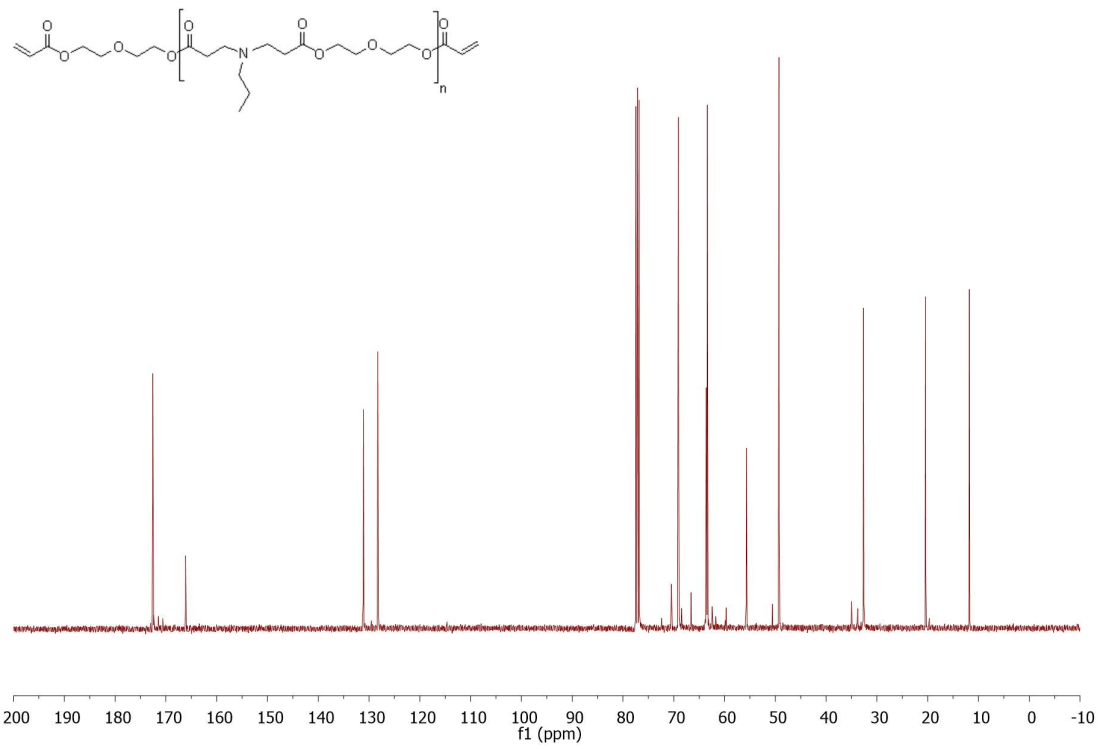

Figure S63. ^{13}C NMR spectrum ($CDCl_3$, 100 MHz) of PBAE *E3*.

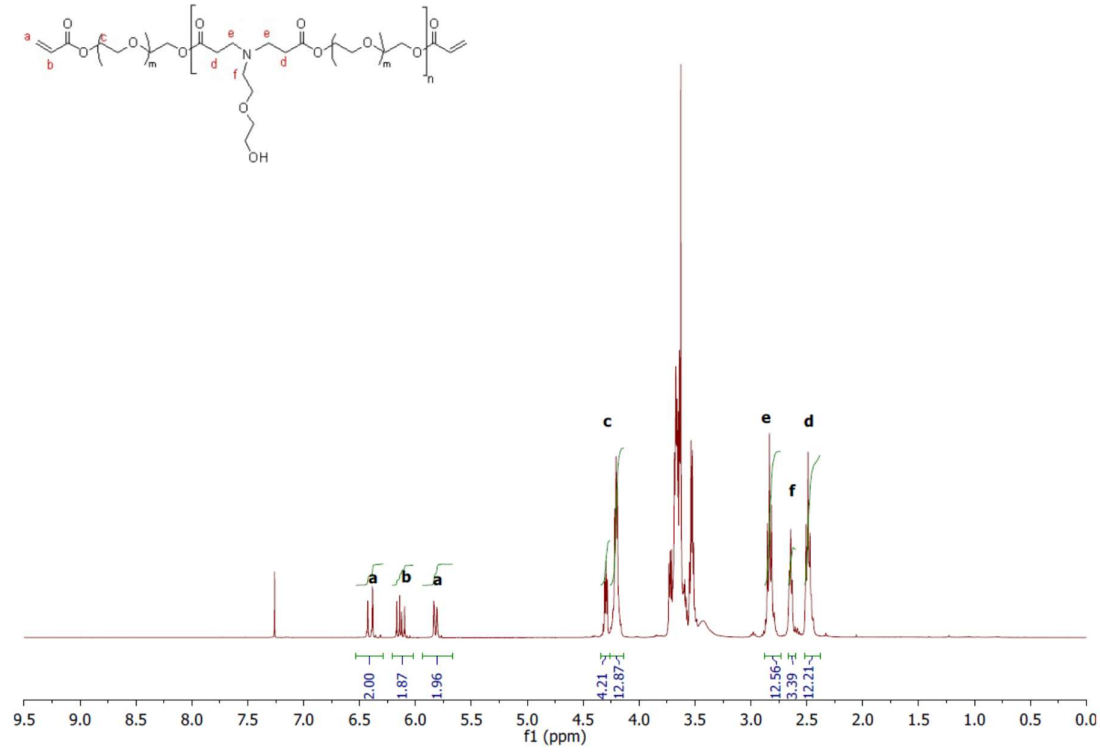

Figure S64. ^{1}H NMR spectrum ($CDCl_3$, 400 MHz) of PBAE *F1* (n=5).

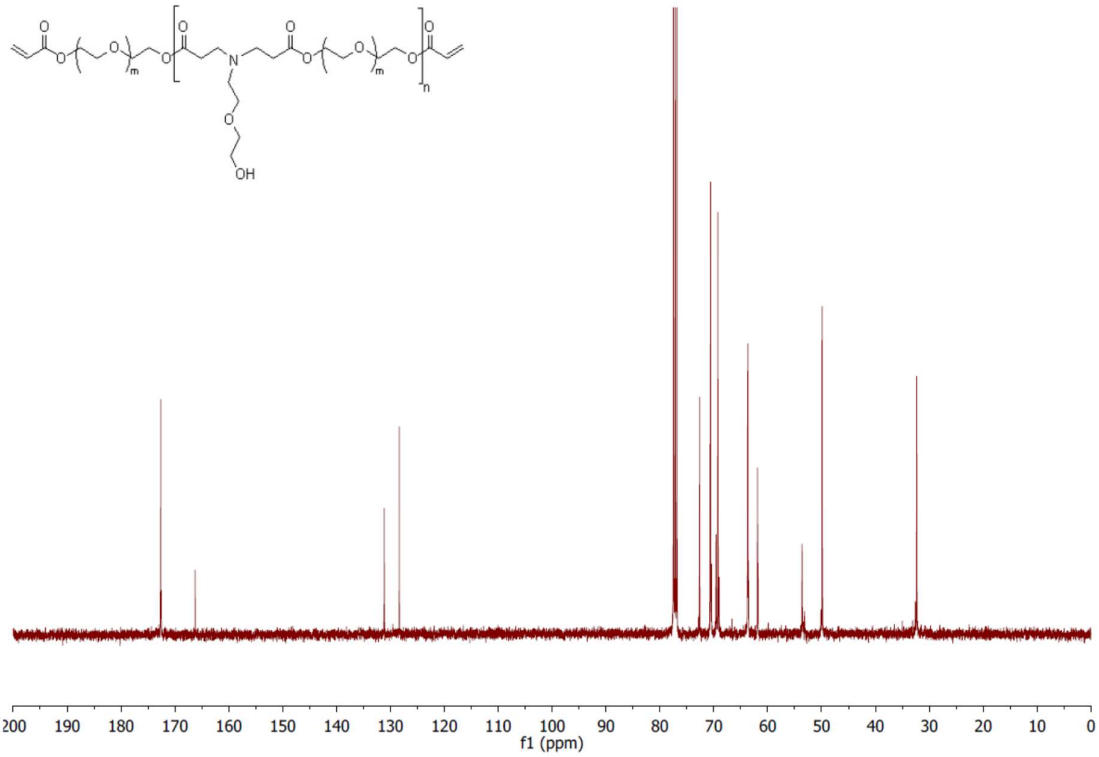

Figure S65. ^{13}C NMR spectrum ($CDCl_3$, 100 MHz) of PBAE *F1*.

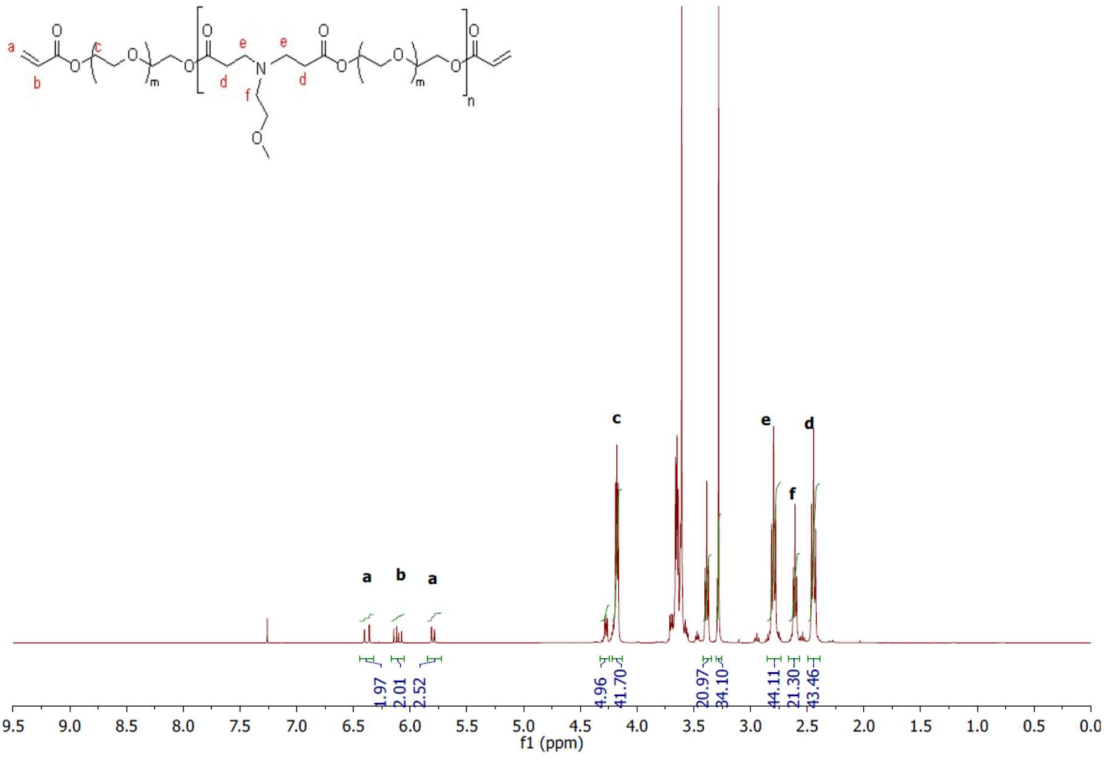

Figure S66. ^{1}H NMR spectrum ($CDCl_3$, 400 MHz) of PBAE *F2* (n= 11).

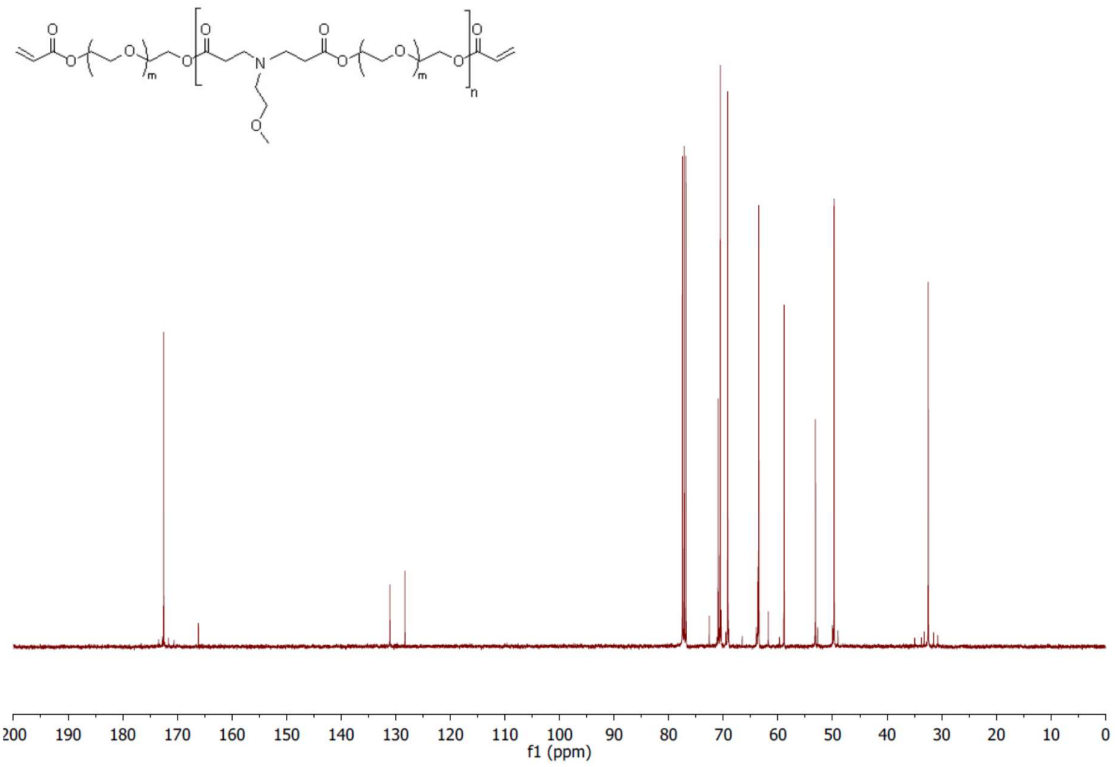

Figure S67. ^{13}C NMR spectrum ($CDCl_3$, 100 MHz) of PBAE *F2*.

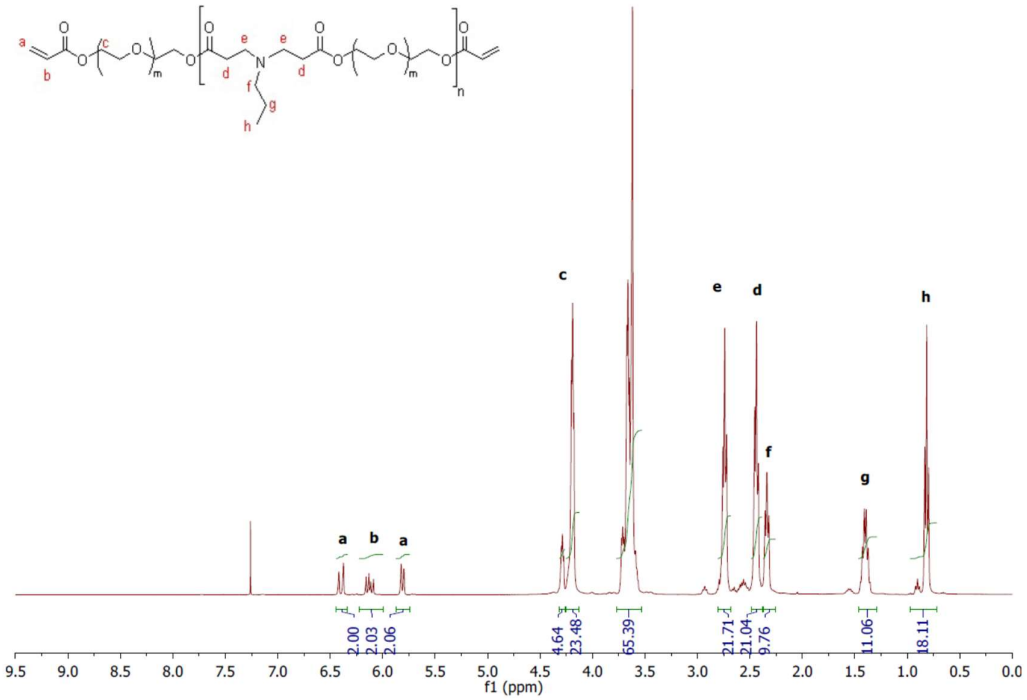

Figure S68. ^{1}H NMR spectrum ($CDCl_3$, 400 MHz) of PBAE *F3* (n= 6).

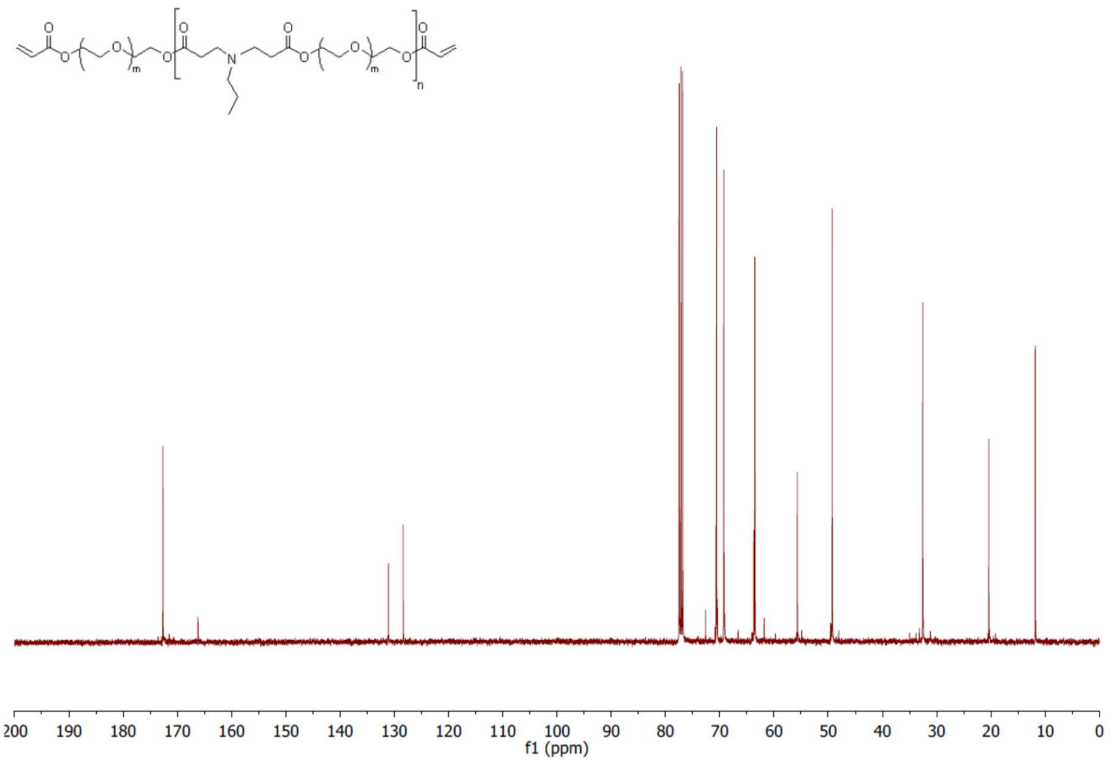

Figure S71. ^{13}C NMR spectrum ($CDCl_3$, 100 MHz) of PBAE *F3*.

S15 Supporting References

(1) Anderson, D. G.; Tweedie, C. A.; Hossain, N.; Navarro, S. M.; Brey, D. M.; Van Vliet, K. J.; Langer, R.; Burdick, J. A. A Combinatorial Library of Photocrosslinkable and Degradable Materials. *Adv. Mater.* **2006**, *18* (19), 2614–2618.

(2) Hook, A. L.; Yang, J.; Chen, X.; Roberts, C. J.; Mei, Y.; Anderson, D. G.; Langer, R.; Alexander, M. R.; Davies, M. C. Polymers with Hydro-Responsive Topography Identified Using High Throughput AFM of an Acrylate Microarray. *Soft Matter* **2011**, *7* (16), 7194–7197.

(3) Dokukin, M. E.; Sokolov, I. Quantitative Mapping of the Elastic Modulus of Soft Materials with HarmoniX and Peak Force QNM AFM Modes. *Langmuir* **2012**, *28* (46), 16060–16071.

(4) Dokukin, M. E.; Sokolov, I. On the Measurements of Rigidity Modulus of Soft Materials in Nanoindentation Experiments at Small Depth. *Macromolecules* **2012**, *45* (10), 4277–4288.

(5) Clifford, C. A.; Seah, M. P. Quantification Issues in the Identification of Nanoscale Regions of Homopolymers Using Modulus Measurement via AFM Nanoindentation. *Appl. Surf. Sci.* **2005**, *252* (5), 1915–1933.

(6) Jee, A.-Y.; Lee, M. Comparative Analysis on the Nanoindentation of Polymers Using Atomic Force Microscopy. *Polym. Test.* **2010**, *29* (1), 95–99.

(7) Butt, H.-J.; Cappella, B.; Kappl, M. Force Measurements with the Atomic Force

Microscope: Technique, Interpretation and Applications. *Surf. Sci. Rep.* **2005**, *59* (1–6), 1–152.

(8) ISO / ASTM52900-15, A. I. ASTM F895 - 11(2016) Standard Test Method for Agar Diffusion Cell Culture Screening for Cytotoxicity, ASTM. 2016, pp 19428–2959.

(9) Borenfreund, E.; Puerner, J. A. Toxicity Determined in Vitro by Morphological Alterations and Neutral Red Absorption. *Toxicol. Lett.* **1985**, *24* (2), 119–124.

(10) Preibisch, S.; Saalfeld, S.; Tomancak, P. Globally Optimal Stitching of Tiled 3D Microscopic Image Acquisitions. *Bioinformatics* **2009**, *25* (11), 1463–1465.

(11) Begines, B.; Hook, A. L.; Alexander, M. R.; Tuck, C. J.; Wildman, R. D. Development, Printability and Post-Curing Studies of Formulations of Materials Resistant to Microbial Attachment for Use in Inkjet Based 3D Printing. *Rapid Prototyp. J.* **2016**, *22* (5), 835–841.

(12) Mandrioli, R.; Mercolini, L.; Ferranti, A.; Furlanetto, S.; Boncompagni, G.; Raggi, M. A. Determination of the Antidepressant Paroxetine and Its Three Main Metabolites in Human Plasma by Liquid Chromatography with Fluorescence Detection. *Anal. Chim. Acta* **2007**, *591* (2), 141–147.